Nano Research

ISSN 1998-0124 CN 11-5974/O4
https://doi.org/10.26599/NR.2026.94909287

Review Article

Mechanism-guided nano and advanced biomaterials for intrauterine adhesions: from pathological microenvironment modulation to functional endometrial regeneration

Jiayi Tian[1,§], Haohan Zhou[2,§], Meimei Zhou[1], Yuan Pan[1](✉)

[1] Department of Prenatal Diagnosis and Reproduction Center, The First Hospital of Jilin University, Changchun 130000, China

[2] Department of Orthopaedic Oncology, Changzheng Hospital, Naval Military Medical University, Shanghai 200003, China

[§] Jiayi Tian and Haohan Zhou contributed equally to this work.

Nano Res., **Just Accepted Manuscript** • https://doi.org/10.26599/NR.2026.94909287

https://www.sciopen.com/journal/1998-0124 on Oct. 26, 2026

© The Authors(s)

Just Accepted

This is a "Just Accepted" manuscript, which has been examined by the peer-review process and has been accepted for publication. A "Just Accepted" manuscript is published online shortly after its acceptance,which is prior to technical editing and formatting and author proofing. Tsinghua University Press (TUP) provides "Just Accepted" as an optional and free service which allows authors to make their results available to the research community as soon as possible after acceptance. After a manuscript has been technically edited and formatted, and the page proofs have been corrected, it will be removed from the "Just Accepted" web site and published officially with volume and article number (e.g., *Nano Research*, **2025**, *18*, 94906990). Please note that technical editing may introduce minor changes to the manuscript text and/or graphics which may affect the content, and all legal disclaimers that apply to the journal pertain. In no event shall TUP be held responsible for errors or consequences arising from the use of any information contained in these "Just Accepted" manuscripts. To cite this anuscript please use its Digital Object Identifier (DOI®),which is identical for all formats of publication.

Just Accepted

Nano Research

Open Access

Review Article

Mechanism-guided nano and advanced biomaterials for intrauterine adhesions: from pathological microenvironment modulation to functional endometrial regeneration

Jiayi Tian[1,§], Haohan Zhou[2,§], Meimei Zhou[1], Yuan Pan[1]✉

[1] *Department of Prenatal Diagnosis and Reproduction Center, The First Hospital of Jilin University, Changchun 130000, China*
[2] *Department of Orthopaedic Oncology, Changzheng Hospital, Naval Military Medical University, Shanghai 200003, China*
[§] *Jiayi Tian and Haohan Zhou contributed equally to this work.*

Received: 8 September 2026; **Revised:** 11 October 2026; **Accepted:** 26 October 2026

✉Address correspondence to panyuan@jlu.edu.cn

Cite this article: *Nano Research*, 2026, 19, 94909287 https://doi.org/10.26599/NR.2026.94909287

ABSTRACT: Intrauterine adhesions arise from failed endometrial repair, in which wound apposition, maladaptive immune–stromal signaling, oxidative injury, fibrotic remodeling and loss of regenerative niches impair reproductive function. This critical narrative review organizes nano and advanced biomaterials around six overlapping biological repair requirements and examines how material structure influences interfacial behavior, mechanics, transport and local exposure. Study-level comparisons distinguish treatment timing, component controls, measured release or residence, and reproductive outcomes. Spatially asymmetric interfaces, stimulus-responsive networks and sequential delivery are evaluated as different design principles; differential release alone does not establish repair-stage matching. Nanoscale structure is also distinguished from evidence that a particular nanoscale feature causes therapeutic benefit. Human evidence is most developed for relatively simple barriers and selected cell–scaffold strategies, whereas catalytic, EV-containing and responsive systems remain predominantly preclinical. We propose minimum sufficient material complexity as a comparison principle: each added component should address a defined unmet function and demonstrate an increment over an indication-relevant simpler approach. Functional recovery requires coordinated hormonal, epithelial, stromal and vascular behavior, with pregnancy outcomes interpreted alongside product fate and reproductive safety.

KEYWORDS: intrauterine adhesion; nanomaterials; biomaterials; extracellular vesicles; endometrial regeneration; reproductive safety

1. Introduction

Intrauterine adhesion (IUA; Asherman syndrome when symptomatic) is a failure of endometrial wound repair in which opposing injured surfaces become connected by scar and the normal epithelial, stromal, glandular and vascular architecture is incompletely restored. Scar-mediated occlusion is accompanied by persistent inflammatory–fibrotic cell states, disrupted epithelial and vascular compartments and altered macrophage–stromal communication in human tissue and single-cell studies [1–3]. Effective treatment therefore combines protection against renewed wall-to-wall adhesion during healing with reconstruction of an endometrium capable of cyclic response, decidualization and safe implantation.

Hysteroscopic adhesiolysis restores cavity access but also creates a fresh wound, so recurrence prevention is an interface-engineering problem. Existing clinical materials show the therapeutic value of physical separation. In a multicenter randomized trial in moderate IUA, a collagen scaffold produced a higher no-recurrence rate at second-look hysteroscopy than an intrauterine device, although changes in adhesion-severity score were not significantly different [4]. A degradable polymer film likewise showed encouraging feasibility after hysteroscopic myomectomy, but its small single-arm design did not provide a controlled estimate of efficacy in recurrent disease [5]. These findings establish simple barriers as the translational benchmark for advanced constructs. Added drugs, nanoparticles, extracellular vesicles (EVs) or cells derive their value from a demonstrable contribution beyond separation alone.

Preventing renewed adhesion does not by itself restore a functional endometrium. A larger randomized study of autologous bone-marrow stem cells on a scaffold plus Foley catheter reported higher ongoing-pregnancy and live-birth rates than Foley-based control, together with an exploratory placental-outcome imbalance described using different labels and analysis populations in the main and sensitivity tables [6]. The signal does not establish treatment causation. A smaller double-blind trial of human umbilical cord-derived mesenchymal stromal cell (hUC-MSC)-loaded collagen scaffold generated a favorable but statistically imprecise live-birth signal [7]. Together, these studies place receptivity, implantation, placentation, live birth and offspring safety alongside recurrence and endometrial thickness as outcomes of regenerative repair.

The uterine cavity imposes distinctive material constraints. Formulations delivered through the cervix need to cover an irregular fluid-exposed surface, avoid bridging the two injured walls and retain their cargo for a defined interval. Temporary barriers, depots and mobile particles require a clear preconception fate, whereas a regenerative implant requires quantified persistence and a biological rationale for safe integration. These demands change with disease stage. Immediately after injury, separation, antifouling and control of excessive inflammation or oxidative and ferroptotic injury may dominate [8]. Profibrotic signaling and matrix remodeling

Just Accepted

become more relevant during fibrotic conversion, while later repair depends on vascular, epithelial, glandular and stromal reconstruction. Persistent indiscriminate immune suppression may disrupt normal wound repair, making temporal control as important as cargo choice [9].

Nano and advanced biomaterials offer several ways to address these coupled constraints. Nanoscale catalysts can provide redox activity, and nanoscale biological vesicles can carry multicargo signals; Ru single-atom and MnO_2 -containing systems and EV-loaded hydrogels or Janus patches illustrate these structures [10–13]. A structural designation, however, does not establish that nanoscale dimensions cause the therapeutic effect. Advanced non-nano hydrogels, ECM scaffolds and degradable films remain essential functional and clinical comparators. Their relative simplicity may confer advantages in manufacturing, sterilization, fate and regulatory control.

Multifunctionality offers potential but also magnifies the evidentiary demands placed on a material. Most intrinsically nanoscale and nano-enabled therapies have been tested in acute rodent injuries treated immediately, often with histology-heavy endpoints and without a strong clinical barrier comparator. Retention is frequently inferred from fluorescence, responsiveness from simplified-buffer assays, and safety from short-term cytocompatibility or maternal-organ histology. EV and cell products add source, potency and batch-variability problems; inorganic nanomaterials add elemental fate and reproductive-system exposure; ECM materials add source and decellularization variability. A sophisticated construct may improve a damaged rodent uterus, yet translation depends on whether its defined structure produces a reproducible increment in the intended clinical scenario and reaches a measured, product-appropriate preconception fate with an adequate reproductive-safety margin.

Recent reviews have addressed IUA mechanisms and exosome–biomaterial innovations, nanomedicine and biomaterials for endometrial regeneration, integrative bioengineering strategies, surgically induced IUA, regenerative biotechnologies and granular hydrogels [14–20]. Building on this literature, we connect disease stage with material function, comparator choice, product definition, fate testing and reproductive safety across primary prevention, recurrence prevention and chronic regeneration.

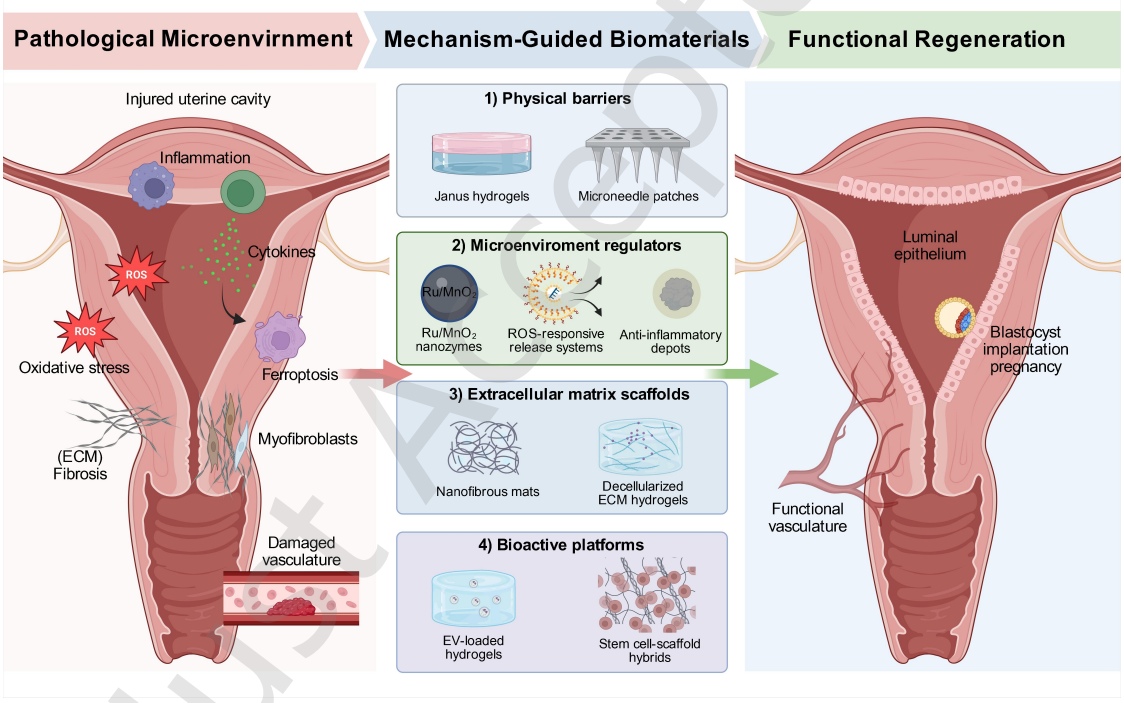


Figure 1. Schematic overview of the pathological microenvironment of intrauterine adhesions, mechanism-guided biomaterial approaches and functional endometrial regeneration. The illustration connects inflammation, oxidative stress, ferroptosis, fibrosis and vascular injury with physical barriers, microenvironment regulators, extracellular-matrix scaffolds and bioactive platforms. The arrows show conceptual therapeutic links, not a validated clinical sequence. ECM, extracellular matrix; EV, extracellular vesicle; ROS, reactive oxygen species.

This critical narrative review draws on targeted PubMed searches, supplementary Google Scholar queries and backward citation tracking through 21 August 2026, supplemented by a targeted revision update conducted on 28–29 September 2026. The update examined sequential delivery, material mechanics and hormone response, immune–stromal regulation, and recent IUA biomaterials; it included full-text assessment of 23 additional candidate reports. This was a targeted expansion, not a rerun of a systematic search. Searches combined IUA, Asherman syndrome or endometrial fibrosis with mechanistic, biomaterial, delivery and regeneration terms. Primary reports were prioritized, and adjacent endometrial or general material studies were identified as indirect. Selection and interpretation were non-systematic; no duplicate screening or formal risk-of-bias assessment was performed. Study comparisons used primary reports and available supplementary material. Heterogeneous models, selective reporting and limited independent replication constrain comparative conclusions.

Biological repair requirements guide the comparison of engineering solutions and the assessment of added material complexity (Figure 1 and Table 1). Table 2 summarizes observed study-level findings. The central question is whether a defined material function improves endometrial recovery beyond an indication-relevant simpler approach.

Just Accepted

2. Biological mechanisms of IUA as design inputs for biomaterials

Within a materials framework, IUA is a temporally evolving failure of endometrial repair in which immune and oxidative stress, fibrotic fixation, and incomplete reconstruction of epithelial, stromal, vascular and reproductive compartments follow injury (Figure 2) [1, 3]. Collagen accumulation represents one component of this process. Patient tissues and human single-cell datasets identify disease-associated states, animal perturbations test causality in vivo, and cell experiments resolve candidate molecular links without reproducing uterine geometry or reproductive function [2, 21]. Table 1 connects these findings with proposed material design considerations and the six overlapping repair requirements in Section 3.

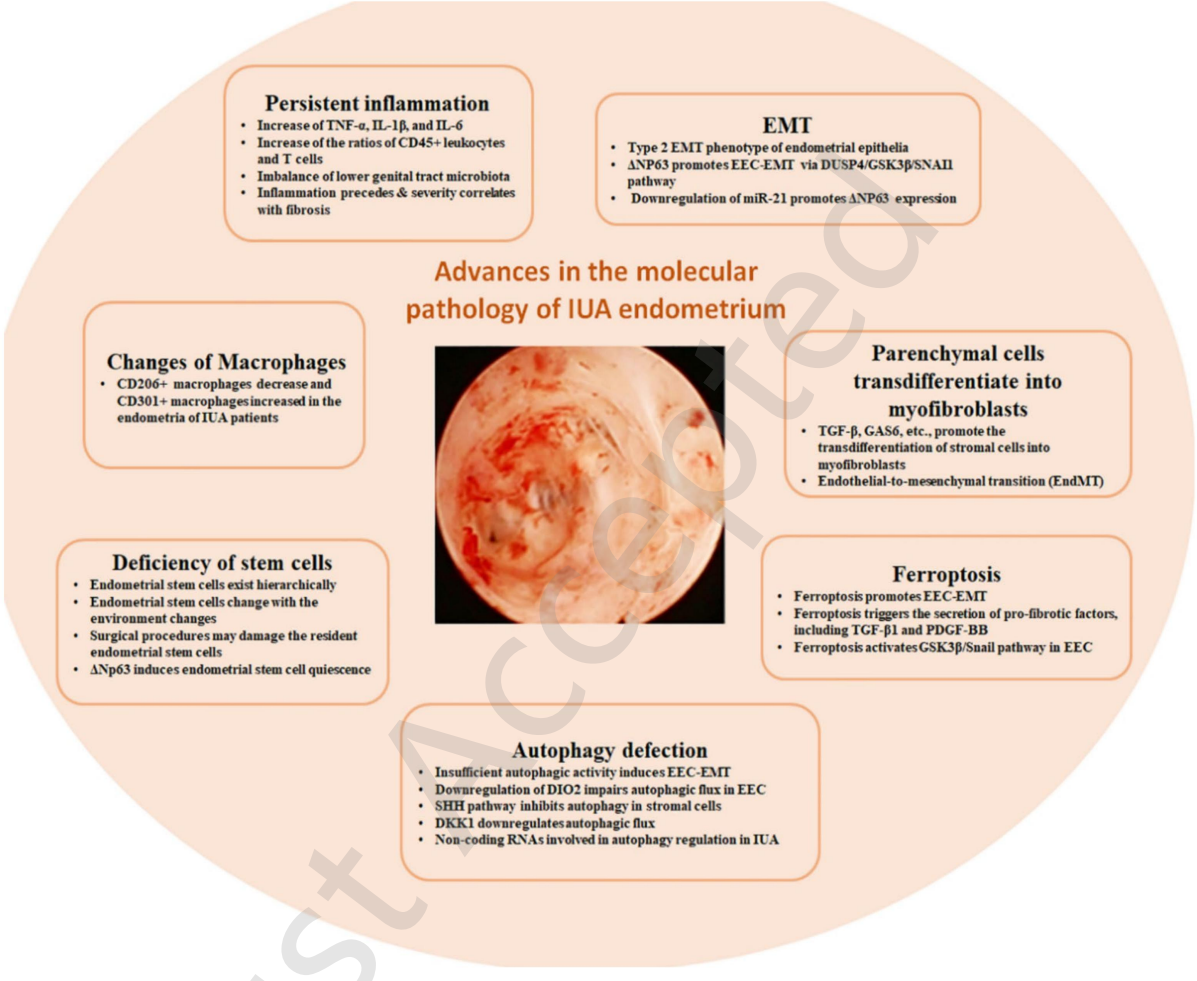


Figure 2. Molecular pathology of the IUA endometrium. The overview integrates persistent inflammation, macrophage-state changes, epithelial- and endothelial-to-mesenchymal transition-like programs, myofibroblast formation, stem-cell deficiency, ferroptosis and defective autophagy. With permission from Springer Nature. [20]

Table 1. Author-proposed links between biological repair requirements, material design variables and evaluable function

Repair requirement / section	Mechanistic rationale	Candidate design variables	Informative functional readouts	Evidence boundary
Separation and epithelial continuity (3.1)	Denuded opposing surfaces and incomplete epithelial closure permit bridging [4, 5, 9, 22].	Coverage, gelation, antifouling, directional adhesion and finite residence.	Coverage and displacement under wet conditions; epithelial closure; recurrent adhesions at second-look hysteroscopy.	Clinical barrier evidence supports separation. A universal human residence period and superiority of a specific advanced interface are not established.
Resolution of immune–stromal signaling (3.2)	Macrophage GAS6–AXL and CCL5/SPP1 can promote stromal activation; early TNF-α can support regeneration in adjacent injury [2, 9, 21].	Local retention, finite immunomodulator exposure and target-linked cargo potency.	Macrophage output together with stromal activation and epithelial recovery; temporal immune-state measurements.	TSG6-EV material evidence supports one implementation [12]. No assumption that every candidate signaling axis already has a validated material therapy; M1/M2 markers alone are insufficient.

Just Accepted

Repair requirement / section	Mechanistic rationale	Candidate design variables	Informative functional readouts	Evidence boundary
Control of oxidative/ferroptotic injury (3.3)	Epithelial/endothelial lipid peroxidation, iron accumulation and inflammatory cell-death programs can amplify fibrosis [8, 23, 24].	Catalytic-site activity, finite antioxidant capacity, iron binding, trigger threshold and exposure duration.	Species-relevant ROS measurements, cell-resolved lipid peroxidation and rescue; vascular function; carrier/element fate.	Catalysis, ROS consumption and ROS-triggered release are distinct. Most therapeutic evidence is acute preclinical injury; short-term organ histology does not establish reproductive safety.
Limitation of fibrosis and maladaptive ECM (3.4)	TGF-β/SMAD, cytoskeletal feedback and stiff-matrix signaling reinforce pathological stromal states [24–27].	Finite drug/siRNA delivery, reversible activity, matrix compliance, degradation and transport.	Target engagement, collagen remodeling and stromal phenotype together with epithelial/gland recovery; evolving mechanics.	An antifibrotic target is not a validated material parameter. Immediate dosing does not prove mature-scar reversal; EMT-like marker changes are not lineage tracing.
Reconstruction of vascular–glandular–stromal niches (3.5)	Loss of epithelial/vascular compartments and stromal competence limits regeneration [3, 22, 28].	Pore connectivity, adhesive ligands, remodeling susceptibility and retained cell/EV/growth-factor activity.	Perfusion and vessel maturity; glandular secretion; epithelial–stromal coordination; cell survival and localization.	CD31 and gland counts are intermediate outcomes. Full-thickness, organoid and direct IUA models address different questions; ECM/cell identity is formulation-specific.
Hormone-responsive reproductive recovery (3.6)	Anatomical repair may not restore coordinated hormone response, decidualization or implantation competence [6, 7, 29, 30].	Ligand–mechanical environment, controlled hormonal exposure and product-specific preconception fate.	Cyclic hormone response and decidualization; implantation, pregnancy, placentation, live birth and offspring follow-up as separate outcomes.	Human-cell models supply adjacent functional evidence [31–35]. Clinical pregnancy/live-birth estimates retain their source populations; no validated universal clearance threshold is proposed.

These links are the authors' conceptual synthesis, not consensus recommendations, regulatory requirements or a validated clinical algorithm. Repair requirements overlap; no universal day ranges are implied. Suggested readouts are prospective design considerations and are not represented as measurements completed by every cited study. ECM, extracellular matrix; EV, extracellular vesicle; IUA, intrauterine adhesion; ROS, reactive oxygen species.

2.1 Basal-layer injury, opposing wound contact and provisional matrix formation

Human single-cell data show severe epithelial loss and disruption of regenerative cell states in IUA, while a mouse full-thickness injury model places epithelial closure before later stromal and gland-associated remodeling (Figure 3) [9, 22, 36]. The clinical benefit of cavity-separating scaffolds and films also identifies wall apposition as a material-relevant target, although those studies do not isolate its biological mechanism [4, 5]. Mouse time-course data establish the sequence of repair but cannot determine how long a barrier should remain in women or after established IUA [9].

Just Accepted

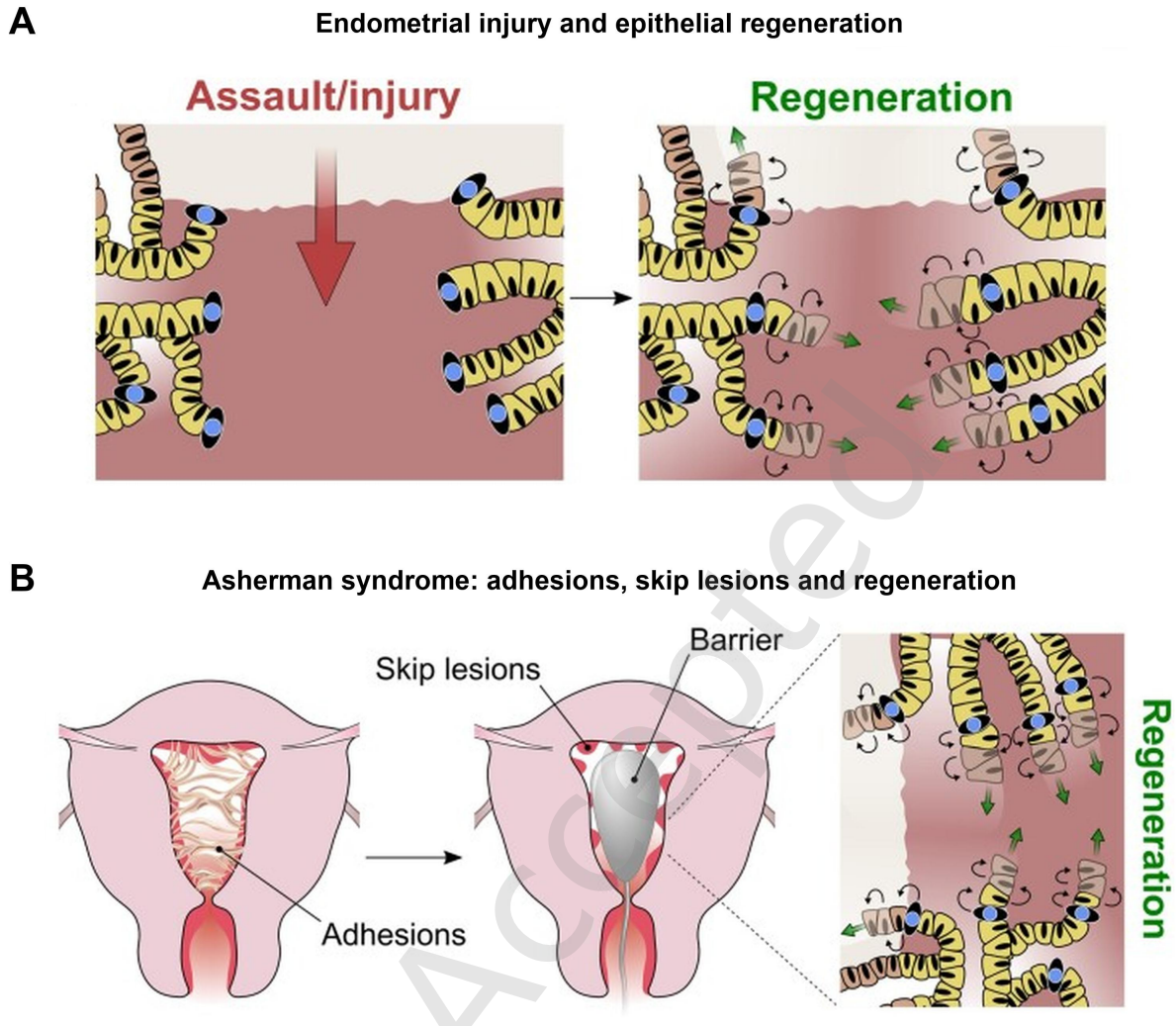


Figure 3. Endometrial gland injury and regeneration. (A) Proposed epithelial regeneration after injury through the basalis gland network. (B) Adhesions, skip lesions, barrier placement and regeneration after adhesiolysis in Asherman syndrome. with permission under the Creative Commons Attribution 4.0 International License (CC BY 4.0). [36]

Human studies have not directly quantified provisional-matrix kinetics, wound–wound apposition or the minimum effective separation period. Early barriers therefore need rapid conformity to the small, irregular and fluid-exposed cavity, resistance to protein and cell attachment at the opposing surface, and sufficient residence to prevent reconnection without blocking epithelial migration [9, 37]. Their residence and degradation can be assessed in relation to re-epithelialization rather than selected for handling convenience alone [9].

2.2 Inflammation, macrophage–stromal crosstalk and infection

Human association and experimental causality converge on persistent inflammatory signaling as a switch from repair to fibrosis [1, 2]. In proliferative-phase patient samples, inflammatory and fibrotic programs coexisted, while sequential mouse sampling showed inflammation preceding fibrosis and stronger disease after curettage plus lipopolysaccharide than after curettage alone [1]. Primed umbilical-cord mesenchymal stromal cells reduced mouse inflammation and fibrosis through complement 1 inhibitor–dependent suppression of a JAK–STAT-associated profibrotic macrophage program, providing in-vivo intervention evidence but not a material-delivery result [1].

The most specific human-to-animal causal chain involves CD301-positive macrophages: single-cell and tissue analyses showed enrichment in IUA, whereas macrophage deletion or AXL inhibition reduced mouse fibrosis and improved pregnancy outcomes; cell studies linked macrophage-derived GAS6 to stromal AXL–NF-κB activation [2]. A separate nine-person single-cell study identified profibrotic macrophage states and confirmed that macrophage-derived CCL5 and SPP1 promote fibroblast-to-myofibroblast transition in vitro [21]. Human single-cell and chromatin-accessibility data further associated SPP1/LGALS9 macrophage networks with multiple fibrotic cell trajectories, although trajectory and ligand–receptor inference do not constitute human intervention evidence [3]. Patient tissue

Just Accepted

and stromal-cell experiments also support LIGHT–HVEM/LTβR as another inflammatory ligand–receptor axis, but no in-vivo blockade was performed [38].

Macrophage effects are phase- and state-dependent rather than adequately described by an M1/M2 binary [2, 9, 39]. CD206-positive cells were reduced in IUA tissue and IL-4-induced macrophage supernatant suppressed TGF-β1-driven stromal fibrosis in vitro, whereas CD301-positive and SPP1-producing states were profibrotic in other datasets [2, 39]. Moreover, in an adjacent mouse injury model, early macrophage-derived TNF-α promoted SFRP4-positive stromal reprogramming and regeneration, cautioning against sustained indiscriminate macrophage or cytokine suppression [9].

The contribution of chronic endometritis to recurrence remains difficult to separate from injury severity and treatment context. Infection-enhanced animal models do not establish a universal infectious driver, so antimicrobial design is most relevant in a prospectively defined infection-risk setting. These uncertainties favor finite immune interventions whose evaluation follows candidate outputs such as GAS6–AXL, CCL5/SPP1 or LIGHT signaling alongside the stromal response [2, 21, 38]. Section 3.2 distinguishes material implementations from still-untranslated target hypotheses and considers preservation of early regenerative immune functions [1, 9].

2.3 Oxidative stress and injury-amplifying cell-death pathways

Ferroptosis is associated with human IUA, whereas therapeutic evidence currently comes from experimental models [8]. RNA sequencing of four severe-IUA and four control endometria, followed by tissue validation, showed enrichment of ferroptosis and lipid-peroxidation signals. Ferroptotic epithelial cells generated profibrotic effects on stromal cells in vitro, and Ferrostatin-1 reduced fibrosis in a dual-injury mouse model [8]. Together, these findings provide convergent patient-association, animal-intervention and in-vitro mechanistic support, while necessity in patients and therapeutic benefit in established disease remain unresolved [8].

Oxidative injury also intersects with other cell-death programs and tissue mechanics [23, 24]. In mice and macrophage cultures, Oroxylin A acted through SIRT3–SOD2–ROS to suppress NLRP3/caspase-1/GSDMD-associated pyroptosis and reduce fibrosis [23]. In a separate mouse-centered study, fibrotic matrix stiffening activated endothelial Piezo1, iron accumulation, lipid peroxidation and ferroptosis, while intrauterine GsMTx4 reduced these changes and fibrosis [24].

These data make ROS-scavenging nanozymes and ROS-cleavable depots plausible approaches to injury-amplifying redox pathways. Their interpretation depends on identifying the target cell and death pathway, demonstrating catalytic or release behavior in uterine fluid, and linking short-term redox control to later tissue restoration [8, 24]. Metal-containing or persistent redox-active systems also raise a distinct fate question in the uterus, ovaries and systemic organs because efficacy markers alone cannot exclude reproductive exposure [24].

2.4 Fibroblast activation, TGF-β/SMAD, epithelial–mesenchymal transition-like changes and ECM deposition

TGF-β/SMAD is the most consistently supported fibrotic hub, although the human evidence is primarily associative [25, 40]. In a 54-patient post-adhesiolysis study, aspirin plus estrogen was associated with lower re-adhesion, reduced fibrotic markers and lower TGF-β1–Smad2/3 activity than estrogen alone, although the small single-center combination design limits causal attribution [40]. In patient tissue, CTRP6 was reduced and inversely associated with fibrosis; CTRP6 overexpression suppressed TGF-β1-induced stromal fibrosis through AMPK/AKT-dependent inhibition of Smad3 in vitro and improved fibrosis in mice [25].

Several experimental modules converge on this hub [26, 41]. Patient tissue, primary epithelial cells and a mouse model linked DIO2 loss and ERK–mTOR-mediated autophagy failure to EMT-like change, with T3 or rapamycin providing partial rescue [26]. In a rat dual-injury model and human epithelial cells, endoplasmic-reticulum stress preceded or amplified TGF-β/SMAD activation and EMT-like markers, while 4-phenylbutyrate or a TGF-β receptor inhibitor attenuated these effects [41]. Human multi-omics indicates that fibrosis involves several stromal, epithelial-like and endothelial-like states communicating with profibrotic macrophages, rather than one uniform fibroblast population [3]. LAMB3–RhoA–ROCK1–MYL9 experiments further connect extracellular-matrix composition to stromal cytoskeletal reorganization, although this mechanism currently has human association plus in-vitro, not animal-intervention, support [27].

Current evidence supports EMT-like and EndMT-like states but not complete epithelial-to-mesenchymal or endothelial-to-mesenchymal lineage conversion [3, 42]. In a rat study, CD31 loss, α-SMA/vimentin gain and CD31/α-SMA colocalization were consistent with an EndMT-like state, although lineage tracing was not performed [42].

Direct human causal evidence for downstream autophagy and ECM-remodeling nodes remains limited, and in the absence of direct perturbation these nodes remain candidate delivery targets. Existing results support testing finite-dose local delivery of small molecules, proteins or nucleic acids during fibrotic conversion, with empty-carrier and cargo-only controls to resolve component contributions [25, 26]. The intended outcome is controlled ECM remodeling and restoration of cell state; prolonged global suppression could also disrupt normal repair [3, 26]. Sections 3.4 and 4.2 therefore consider biochemical exposure and evolving matrix mechanics together, without inferring a validated therapeutic modulus from mechanistic association.

2.5 Vascular, glandular and stem/progenitor-cell niche failure

Vascular failure appears mechanistically coupled to fibrosis [24, 28]. VEGF165 was lower in patient Asherman endometrium, and experimental VEGF reduction produced fibrosis in mice; in primary stromal cells, VEGF165 inhibited TGF-β1-driven α-SMA and collagen through DLL4–Notch4–SMAD7 [28]. Matrix stiffness–Piezo1–ferroptosis provides an additional animal and cell mechanism by which a fibrotic matrix can deplete or disable endometrial endothelial cells [24].

Human single-cell evidence also indicates broader regenerative-niche disruption [3, 22]. Severe-IUA samples showed extensive epithelial injury, loss of MMP7-positive and CCL5-positive nonciliated epithelial subpopulations, inflammatory macrophage activation and ECM-rich fibroblast programs, although only four IUA donors were profiled [22]. Human multi-omics resolved several fibrotic trajectories, leaving permanent exhaustion of a single stem-cell population unproven [3]. In an adjacent mouse injury model, SFRP4-positive stromal cells underwent TNF-α/EHF-dependent developmental reprogramming and improved regeneration after transplantation, supporting regenerative

Just Accepted

competence as a manipulable state without demonstrating treatment of established human IUA [9].

Direct human evidence linking endothelial senescence or specific epithelial WNT/Notch states to material-responsive repair remains limited. Regenerative scaffolds can nevertheless combine ECM-mimetic architecture with local retention of cells, EVs or growth factors, while pore structure, fiber organization, mechanics and degradation influence the environment for epithelial, glandular and vascular reconstruction [9, 22]. Increased CD31 or in-vitro tube formation indicates a vascular response, not stable perfusion. Section 3.5 evaluates whether the chosen architecture restores connected tissue functions rather than marker abundance alone.

2.6 Failure of receptivity and decidual function

Functional receptivity encompasses more than anatomical recovery or endometrial thickness [29, 40]. After TCRA and the same estrogen regimen, five thickness-defined responders and five nonresponders showed distinct epithelial, stromal and immune single-cell states; the unpaired exploratory design leaves the cause of estrogen resistance unresolved [29]. Estrogen effects were also context- and dose-dependent in primary epithelial cells and an animal model: a concentration that inhibited proliferation in normal cells attenuated TGF-β1-associated EMT-like change in fibrotic conditions [30]. The aspirin-plus-estrogen study improved short-term thickness and re-adhesion measures without establishing live-birth benefit or long-term reproductive safety [40].

Available human studies have not yet defined an IUA-specific window-of-implantation signature or demonstrated a causal defect in decidualization. Evaluation of regenerative systems should therefore distinguish thickness, gland counts, Masson staining and CD31 from cyclic hormone response, coordinated epithelial–stromal behavior, decidualization, implantation and pregnancy outcomes [22, 29]. Section 3.6 uses adjacent human-cell and organoid models to clarify these functional tests without treating them as IUA efficacy evidence. Product-specific preconception fate and quantified persistence remain relevant, and short-term histology or implantation counts cannot establish placental, fetal or offspring safety [6].

3. Biomaterial interventions organized by biological repair requirements

The six repair requirements below provide a common organizing principle for the mechanisms in Section 2 and the engineering solutions evaluated here. They can coexist within one lesion; their order is not a validated clinical staging system or a fixed release timetable. Each intervention is interpreted according to its injury model, treatment timing, component controls and measured outcome. Table 2 consolidates representative study-level observations. Hydrogels, fibers, EVs and cells are treated as possible means of meeting a requirement, rather than mutually exclusive therapeutic categories.

3.1 Preventing wound apposition and restoring epithelial continuity

After injury or adhesiolysis, the immediate engineering task is to separate denuded walls while permitting epithelial closure. A material that binds equally strongly to both surfaces may itself form a bridge; a completely nonadhesive formulation may wash out before repair. Thus cavity coverage, directional fixation and finite residence matter more than the material-class label. Clinical gels, films and collagen scaffolds provide the relevant non-nano benchmarks [4, 5, 43–46]. The indication must remain explicit: placement after myomectomy tests primary prevention, whereas placement after adhesiolysis tests recurrence prevention in previously scarred tissue.

In a multicenter randomized trial, an in-situ-forming hydrogel improved adhesion-free status at eight weeks, including in the adhesiolysis subgroup, but did not establish reproductive benefit or measure intrauterine residence [46]. A collagen scaffold also improved the no-recurrence outcome relative to an intrauterine device, although changes in AFS severity score did not differ [4]. In a separate randomized hyaluronan study, clinical-pregnancy and implantation analyses were conditional on embryo transfer; differential transfer cancellation prevents interpreting those percentages as outcomes among all randomized women [45]. Observational collagen- and hyaluronan-gel studies, the PREG1 film-feasibility study, and silicone, amnion or oxidized-cellulose barriers broaden the deployment experience without establishing one universally superior product [5, 43, 44, 47–50].

Advanced interfaces address specific shortcomings of separation alone. Granular hydrated and zwitterionic hydrogels combine injectability with resistance to nonspecific adsorption [37, 51]. Microfluidically templated porous scaffolds introduce a controllable void structure for local delivery, but fabrication tunability should not be confused with an isolated pore-size effect on fertility [52]. Arrowhead composite microneedles partition tissue attachment and luminal protection (Figure 4) [53]; Janus microgels and microstructured bioadhesives similarly allocate anchoring and anti-adhesion to different faces [54, 55]. An EV-loaded Janus adhesive microneedle patch combines directional fixation with vesicle delivery in experimental IUA [13]; its release measurements are considered separately in Section 4.3. For the microstructured bioadhesive, abdominal and uterine adhesion results are distinct experiments, and neither establishes a human residence interval. These are examples of spatial allocation, not sequential treatment.

Just Accepted

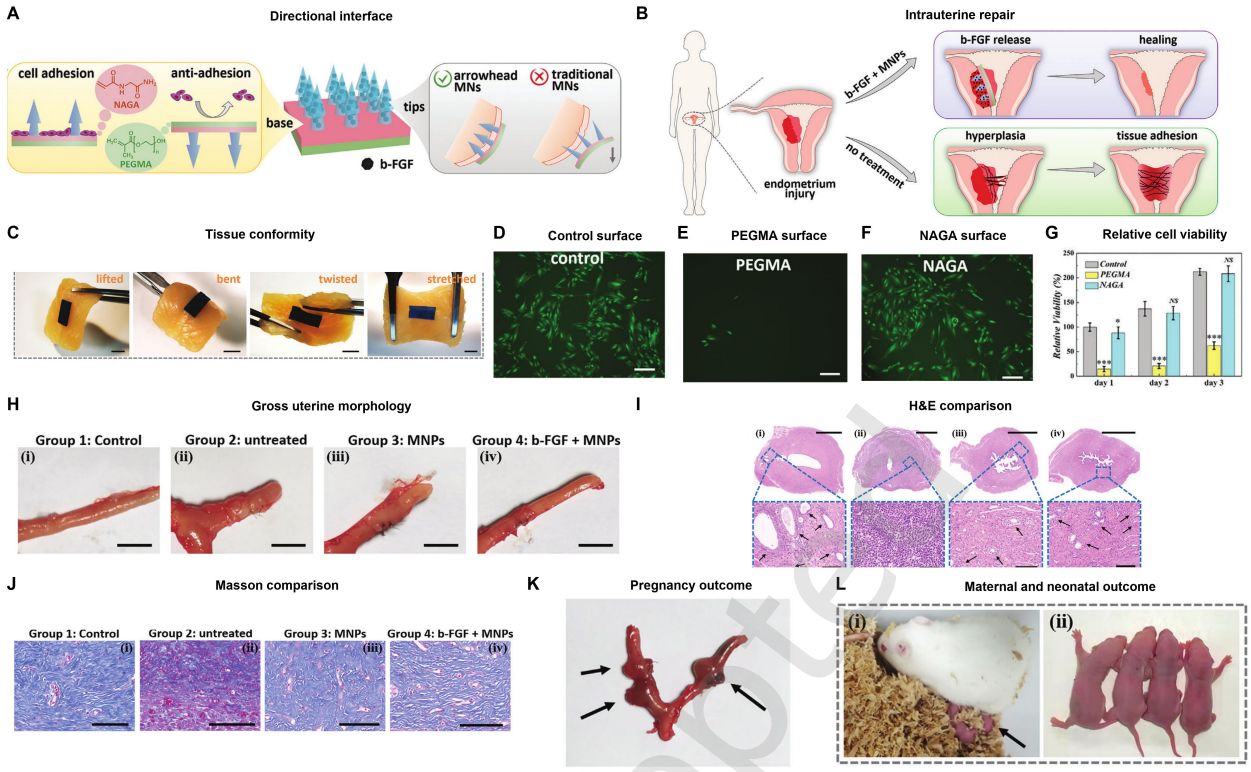


Figure 4. Arrowhead composite microneedle patches with anisotropic surface adhesion. (A,B) Directional interface design and intrauterine b-FGF delivery; (C) tissue conformity; (D–G) surface-specific cell adhesion and viability; (H–J) gross uterine morphology, H&E and Masson staining; and (K,L) pregnancy and maternal–neonatal outcomes. with permission under CC BY 4.0. [53]

An active interface can also influence the injured surface. VEGF-bearing anti-inflammatory films, mechanically robust estradiol barriers, PRP hydrogels and amorphous-curcumin formulations couple separation with local signaling [56–61]. For these drug-loaded systems, an empty-material comparison helps distinguish barrier behavior from cargo activity. A pH/ROS-responsive antifouling PEG hydrogel instead incorporates antioxidant chemistry into the network itself [62]. Its vehicle comparison does not separate physical separation and antifouling from reactive-group ROS consumption or responsive degradation. Reproductive assessment involved three female rats per group with paired healthy and injured horns; relative embryo numbers improved, without establishing an absolute implantation rate, live-birth rate or reproductive safety [62].

3.2 Resolving maladaptive immune–stromal signaling

The material target is persistent profibrotic communication, not inflammation in the abstract. The GAS6–AXL and CCL5/SPP1 findings in Section 2 identify macrophage outputs and stromal responses that could be measured together, whereas the reparative TNF-α–SFRP4 interaction cautions against prolonged, indiscriminate suppression [2, 9, 21]. LIGHT–HVEM/LTβR remains a candidate delivery target supported by patient tissue and stromal-cell experiments without in-vivo blockade in the cited study [38]. CTRP6 has cellular and mouse antifibrotic evidence, but that evidence does not validate a CTRP6-delivering biomaterial [25]. These target hypotheses should therefore be distinguished from the tested material implementations below. A depot needs to control the location and duration of bioactivity while allowing early repair signals to recover; CD86/CD206 changes alone cannot demonstrate interruption of a specific macrophage-to-stromal pathway.

The TSG6-engineered EV thermogel provides a relatively direct example of this connection (Figure 5) [12]. Its mechanistic experiments linked inhibition of macrophage activation with reduced stromal myofibroblast activation; the material arm compared empty chitosan/β-glycerophosphate gel, control-vector EV gel and TSG6-EV gel. A 2% chitosan formulation degraded almost completely over nine days in lysozyme-containing buffer, while a separate fluorescent tracking experiment compared free and gel-bound EV retention through seven days at 50 μg EV protein. These observations support engineered-cargo activity and a carrier-associated residence effect, while the independent contribution of EV nanoscale dimensions remains unresolved. Translation of the day-14 murine tissue outcomes to a chronically scarred human uterus also requires evidence of the necessary local exposure [12].

Just Accepted

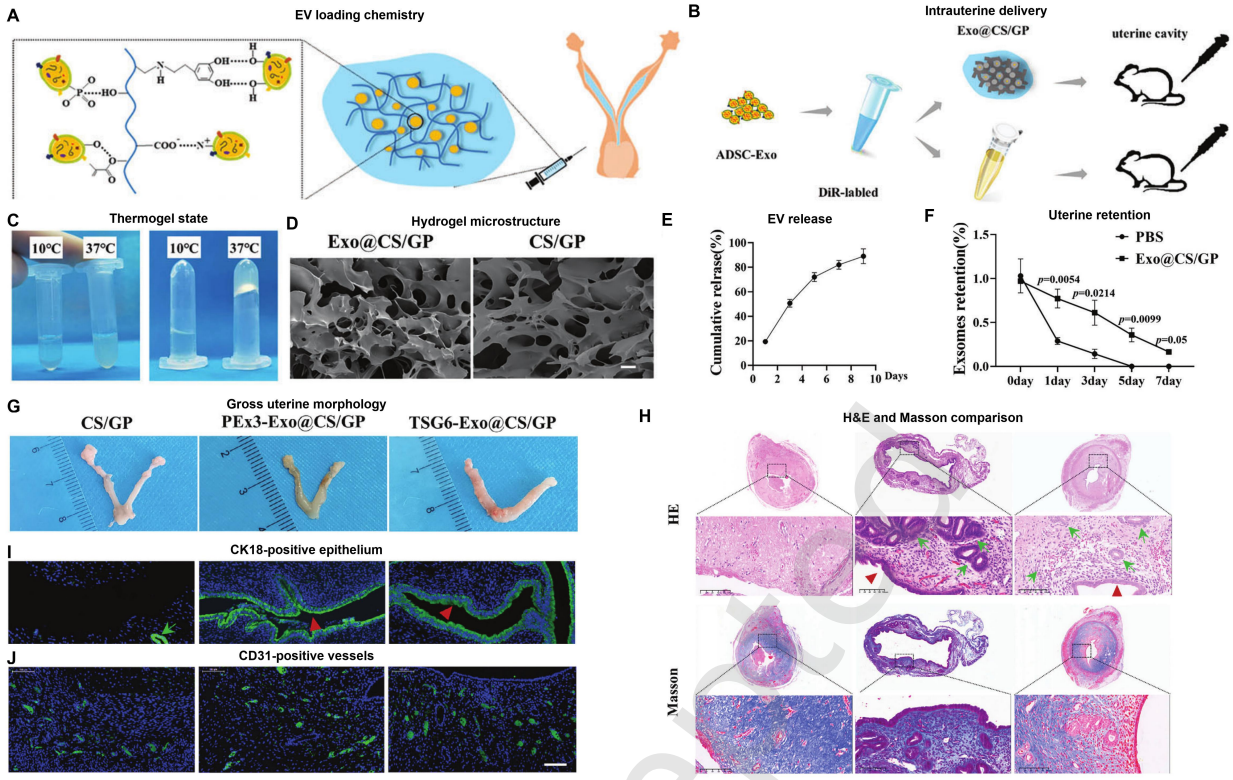


Figure 5. TSG6-engineered extracellular vesicles delivered in a chitosan/β-glycerophosphate thermogel. (A,B) EV-loading chemistry and intrauterine delivery; (C–F) thermogel transition, hydrogel microstructure, EV release and uterine retention; and (G–J) gross morphology, H&E/Masson, CK18 and CD31 outcomes. With permission from Wiley-VCH GmbH. [12]

Other systems emphasize the connection between attachment, cell retention and paracrine signaling. A mussel-inspired, visible-light-crosslinked hydrogel carrying umbilical-cord MSCs compared free cells with cells in methacrylated hyaluronic acid and its dopamine-modified counterpart; the animal efficacy series did not include a cell-free hydrogel arm [63]. Cell-associated fluorescence persisted through day 14 only in the dopamine-modified group, supporting improved label persistence rather than quantifying surviving therapeutic cells. Dopamine modification changes several interface and network properties together, so a macrophage response cannot be assigned to stiffness alone. Thermosensitive EV depots likewise require separation of cargo potency from carrier effects [64]. TNF-α-primed MSC work is mechanistically informative, yet its animal treatment used the primed cells, not an isolated EV–material product [65].

Immune modulation should be evaluated against persistent stromal states as well as cytokine panels. The TNS1/TAGLN-enriched stromal-cell study identifies a candidate fibrotic state through public-cohort reanalysis and experimental phenotype validation; its gene perturbations were computational [66]. These observations are not an independent new human cohort or proof that an existing hydrogel selectively removes that state. Antimicrobial functions address a separate, infection-defined indication. Silver-containing nanostructures with in-vitro antibacterial findings are not evidence of animal IUA treatment, and a Lactobacillus-loaded depot introduces viability and host-interaction variables beyond those of a conventional polymer gel [67, 68]. Neither infection-enhanced injury nor broad cytokine reduction justifies routine antimicrobial loading in every IUA construct.

3.3 Limiting oxidative and ferroptotic injury

Oxidative injury can damage epithelium and endothelium and reinforce stromal fibrosis. Three engineering mechanisms should be distinguished: catalytic conversion of ROS, finite chemical consumption of ROS, and ROS-triggered changes in carrier behavior. A fourth route regulates the cell's own antioxidant machinery. These mechanisms can coexist, but they differ in dose definition, capacity, duration and the controls required for attribution [8, 10, 11, 69, 70].

Ru single-atom nanozymes couple atomically dispersed catalytic architecture to redox and ferroptosis-related activity in rodent endometrial injury (Figure 6) [10]. Hollow MnO_2 -containing hydrogels provide another catalytic composite: the study reported 86.5% ABTS scavenging for HME200 and injured-right-horn pregnancy of 45.5% with HME versus 9.1% with natural repair (11 females per group) [11]. These measurements link formulation to antioxidant activity and an animal reproductive outcome, but the in-vitro radical assay does not measure catalytic exposure in uterine fluid. Likewise, the reproductive comparison does not isolate nanoscale geometry from manganese chemistry, cargo or gel retention.

Just accepted

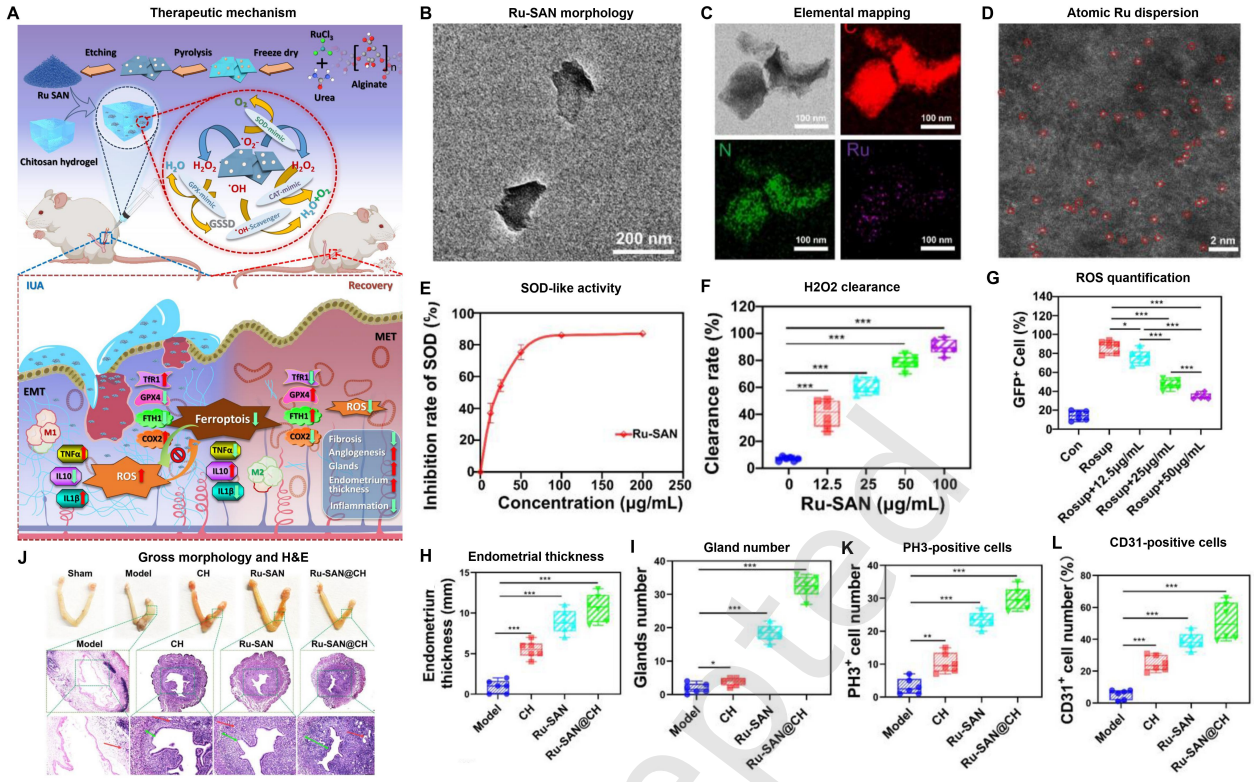


Figure 6. Ru single-atom nanozyme hydrogel targeting ROS–ferroptosis-associated injury. (A) Ru-SAN fabrication, hydrogel delivery and proposed therapeutic mechanism; (B–G) morphology, elemental mapping, atomic Ru dispersion, catalytic activity and ROS quantification; and (H–L) uterine morphology, endometrial thickness, gland number, proliferation and vascular outcomes. with permission under CC BY 4.0. [10]

A newer cerium–tannic-acid nanozyme hydrogel combines measured SOD-/CAT-like activity with a ROS-responsive network [71]. By day 8, TA-based release was 96.87% in 0.03% H_2 O_2 versus 53.67% in PBS; this in-vitro assay does not quantify intact active nanozyme release or sustained catalytic turnover in vivo. Conversely, a ROS-responsive iron-trapping hydrogel targets the hemorrhage–iron–lipid-peroxidation sequence without being a nanozyme [72]. This distinction changes the design question: removing a source of iron-dependent injury is not equivalent to catalytically converting ROS after they form. Both approaches remain experimental injury interventions; improvement after early dosing is not proof of mature-scar reversal.

EV-mediated Nrf2/GPX4 regulation instead engages endogenous antioxidant defenses [69]. Thiol-rich networks and pH/ROS-sensitive antifouling gels can consume oxidants or change their own chemistry while also acting as barriers [62, 73]. Their finite reactive capacity should not be described as sustained enzyme-like turnover without catalytic measurements. Multiresponsive microcapsules illustrate a further combination of externally responsive release and composite bioactivity (Figure 7) [74]. The accessible main study did not provide a composition- and mechanics-matched nonresponsive comparator, so therapeutic effects cannot be assigned solely to responsiveness.

Just Accepted

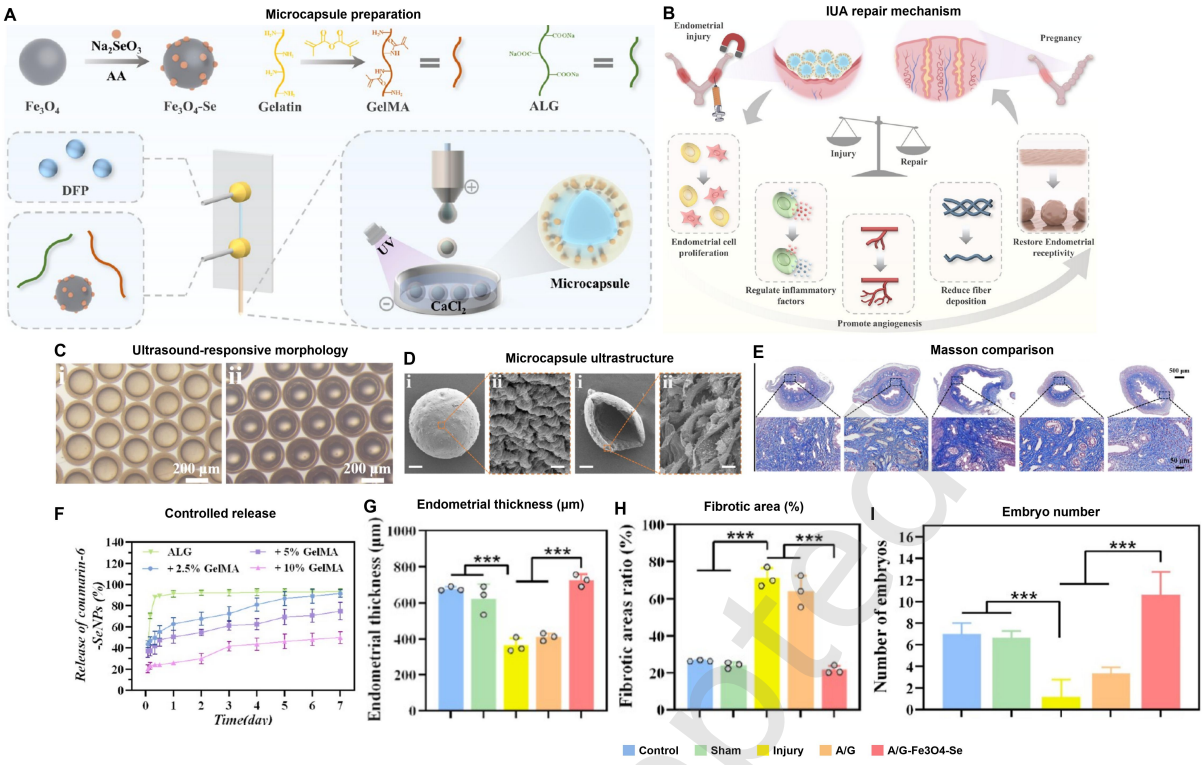


Figure 7. Multiresponsive microcapsules for intrauterine adhesion prevention. (A,B) Fe3O4–Se synthesis, coaxial-microfluidic fabrication and the proposed repair mechanism; (C,D,F) ultrasound-responsive morphology, microcapsule ultrastructure and controlled release; and (E,G–I) Masson staining, endometrial thickness, fibrotic area and embryo number. With permission from the American Chemical Society. [74]

Across these systems, the relevant biological readout depends on the intended target: epithelial or endothelial lipid peroxidation and rescue experiments address ferroptosis, whereas macrophage inflammasome and gasdermin measurements address pyroptosis [8, 23, 24]. Suppression of bulk tissue ROS cannot resolve either pathway on its own. Retained activity in protein-containing fluid, local dose and persistence are particularly important for catalysts because the therapeutic window may end before the material disappears. The evidence supports preclinical redox intervention, while nanoscale-feature dependence and preconception elemental fate remain separate questions.

3.4 Interrupting fibrotic signaling and maladaptive matrix remodeling

Persistent TGF-β/SMAD signaling and altered ECM–cell feedback provide a rationale for a finite local antifibrotic exposure. The objective is to reduce pathological matrix fixation while preserving the remodeling needed for epithelial and stromal recovery. Thus the useful material variables are drug availability, cellular uptake, burst release, matrix compliance and reversibility, rather than maximal suppression of a fibrosis marker [24–27].

A sodium-hyaluronate siSMAD3 hydrogel links sustained nucleic-acid delivery to uptake and target knockdown [75]. A pH-responsive carrier for integrin α5β1 agonism connects local delivery with osteopontin-associated fibrosis and includes tracking of free versus hydrogel-encapsulated labeled liposomes [76]. These comparisons inform retention or target activity, but a matched pH-insensitive matrix would be needed to isolate the trigger itself. An antioxidant vericiguat depot adds a pharmacological route involving sGC/cGMP/SMAD7 signaling [77]. Treatment began three estrous cycles after rat injury, with local free-drug and loaded-gel arms each receiving a nominal 2-mg dose, alongside empty-gel and oral-drug controls. Approximately 15% release by day 3 was measured in surfactant-containing buffer, while about 20% gel mass remained intrauterine at day 15; these are different measures of drug transport and carrier persistence. This delayed design is more informative for established injury than immediate dosing, but does not by itself document reversal of a mature adhesion. Patient tissue supplies disease context, not clinical evidence for hydrogel treatment, and sGC perturbation does not establish that SMAD7 is required for every observed effect.

The decidualized-ECM/Tβ4 construct combines matrix-derived cues with PLGA microsphere delivery (Figure 8) [78]. Loaded microspheres averaged 35.6 μm, placing the reported depot at the microscale rather than establishing a nanoparticle effect. Microspheres alone released nearly 70% of Tβ4 within three days in vitro; incorporation in ECM reduced the burst and extended release over the ten-day assay. This demonstrates altered transport by a second matrix, not superiority of sequential over simultaneous therapy. The report also presents implantation and offspring outcomes, although unresolved differences between the stated gestational-day-19 collection method and the live-birth/offspring descriptions limit interpretation of these observations as an unqualified live-birth rate [78].

Just Accepted

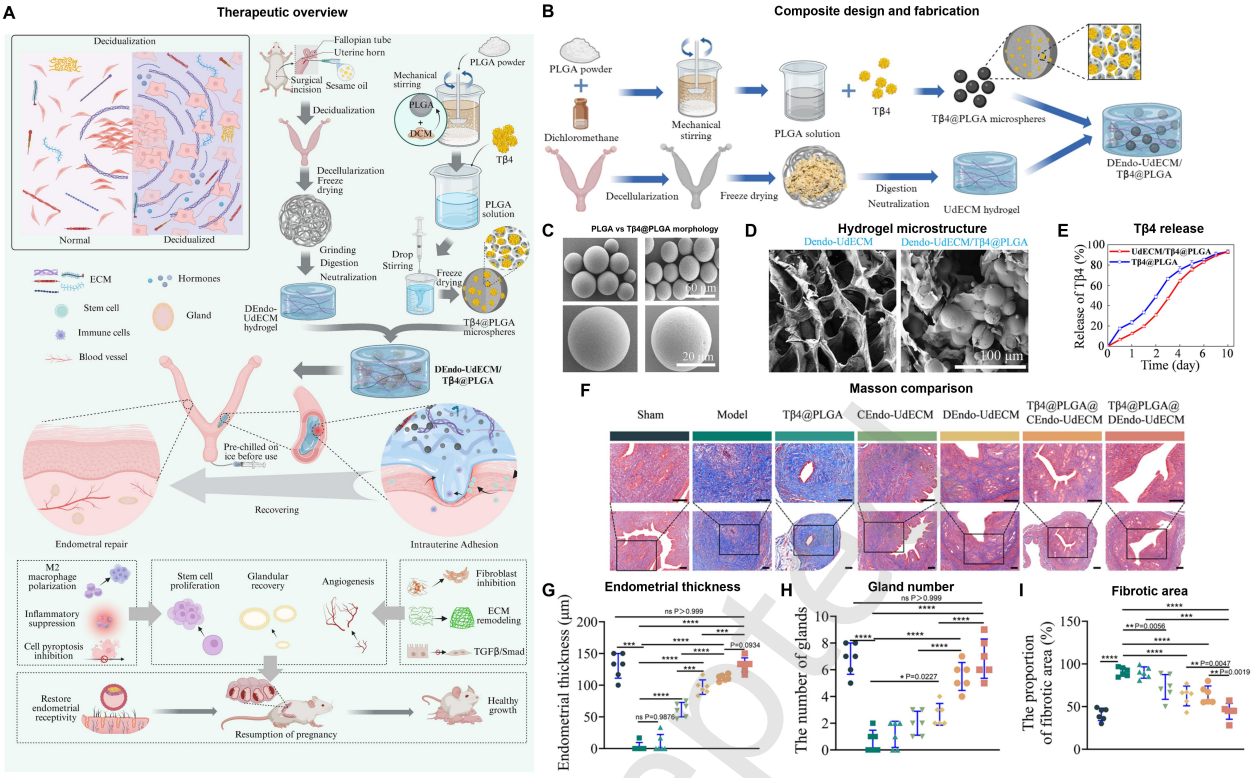


Figure 8. Decidualization-empowered endometrial ECM hydrogel with sustained thymosin β4 delivery. (A,B) Therapeutic overview and construct fabrication; (C–E) microsphere and hydrogel morphology and Tβ4 release; and (F–I) Masson staining, endometrial thickness, gland number and fibrotic area. with permission under CC BY 4.0. [78]

Micro–nano composites can add another level of delivery control. Pirfenidone-loaded polydopamine nanoparticles combined with cell-bearing GelMA/HAMA microspheres test microenvironment modulation and cell support in the same construct [79]. The reported particles were approximately 310 nm and the microspheres 279 μm. Comparisons with free cells and cell-bearing microspheres inform the combination, but absent empty-microsphere, free-pirfenidone and drug-free-polydopamine efficacy arms leave component attribution incomplete. A strontium/betamethasone–oxidized-alginate hydrogel provides a separate non-nano formulation benchmark in which ionic crosslinking, drug loading and network behavior are coupled [80]. Its anti-inflammatory effects are not equivalent to demonstrated blockade of a specific macrophage–stromal circuit.

Mechanobiology adds a complementary target, but evidence for a target is not evidence for a mechanically optimized therapy. The Piezo1 study links stiff matrix conditions to endothelial ferroptosis [24]. In a separate report, miR-195-5p agomir treatment beginning seven days after injury showed antifibrotic activity, with cellular Smad7 knockdown supporting a Smad7-dependent component [81]. This does not establish the complete directional YAP–Smad7 pathway, an EV hydrogel or a stiffness-directed treatment. Together with persistent TNS1/TAGLN-associated stromal states [66], these findings motivate testing matrix mechanics and cell state during degradation. They do not define a universal antifibrotic modulus or prove reversal of a documented mature adhesion.

3.5 Reconstructing vascular, glandular and stromal niches

Once opposing surfaces are protected, tissue repair depends on restoring connected epithelial, vascular and stromal compartments. Scaffold geometry, ligand presentation and transport can support this task, while cells, growth factors and EVs provide different sources of signaling. CD31 staining and gland counts describe tissue composition; perfusable vessels, glandular secretion and coordinated epithelial–stromal responses answer more functional questions [22, 28].

Sequential VEGF/IGF-1 delivery was designed to combine early vascular support with subsequent tissue reconstruction [82]. This study provides a more specific temporal delivery example than grouping all multifunctional constructs together; Section 4.3 examines its actual comparator and release evidence. Injectable 3D-printed porous scaffolds carrying adipose stem cells address another constraint: a regenerative construct must retain viable cells yet pass through a limited delivery route [83]. Treatment began one week after scraping/LPS injury, and the study compared blank scaffold, free cells or exosomes, and their scaffold-loaded counterparts. Porous versus nonporous architecture was characterized, but not isolated in a cell-matched animal efficacy comparison. Thus post-injection recovery, porosity and cargo support remain related contributors rather than proof of a pore-size-specific reproductive benefit.

Nanofibrous silk-fibroin/polycaprolactone mats provide an ECM-like cell-supporting architecture in rat injury [84]. This is a structural description; without a matched nonfibrous material it does not establish dependence of repair on nanofiber dimensions. SDF-1α-bearing fibrous or collagen constructs recruit reparative cells, offering an alternative to transplanting a manufactured cell product [85, 86]. Uterine ECM, urinary-bladder matrix, amniotic-derived gels and injectable short fibers supply different combinations of ligands, shape and retained cues [87–91]. This group provides preclinical repair evidence across different injury and formulation settings; its tissue or reproductive endpoints

cannot isolate a shared ligand or fiber mechanism. The rabbit electrothermal-injury membrane study broadens the injury context [90]. Printed constructs and ECM/cell hybrids further span uterine-wall reconstruction and intrauterine repair [92–96]; full-thickness defect restoration addresses a different anatomical problem from preventing opposing denuded surfaces from re-adhering.

The composition of the regenerative niche can be tested in more defined systems. Fully synthetic matrices supporting human endometrial organoids and epithelial–stromal co-cultures allow adhesive ligands and degradability to be specified [34, 97]. These are functional models, not IUA treatments. In contrast, a microfluidic vascularized endometrial complex was transplanted during ethanol injury in immunodeficient mice [98]. Its fibrin/Matrigel formulation changes matrix chemistry as well as mechanics, while adding endothelial cells also reduces the stromal-cell fraction. Subcutaneous graft perfusion is not evidence of restored maternal placental circulation, and inconsistent laterality definitions limit interpretation of the reported horn-based reproductive percentages. Multilineage organoids on acellular amniotic membrane were studied in rat repair [99]. The embryo-count analysis selected three mated rats per group, and its organoid-versus-organoid/patch comparison was nonsignificant. These studies support multicellular repair strategies without establishing an independent fertility gain from every added scaffold component.

Cell and EV constructs should be chosen for their biological contribution rather than assumed interchangeability. Menstrual-blood stromal-cell EVs improved rat endometrial thickness but did not equal cell treatment at the latest assessment [100]. Protective EV hydrogels and matrix/collagen/fibrin carriers provide experimental evidence of repair and, in some studies, reproductive outcomes [101–104]. Such efficacy supports the tested formulation; it does not establish a common retention mechanism without matched exposure measurements. EV-producing microfibers and an EV/spermidine hydrogel also alter the biological production environment or delivered cargo, limiting attribution to the carrier alone [105, 106]. Apoptotic bodies have different biogenesis and size distributions from small EVs [107]; EV terminology otherwise follows MISEV2023 unless endosomal biogenesis has been established [108].

Cell–gel, cell–amniotic-membrane and cell–collagen studies provide animal repair or feasibility evidence using different cell sources, doses and injury settings [109–116]. These comparisons remain informative within each experiment, while isolated scaffold, cell-survival and reproductive effects cannot be ranked across the group. The PRP/ADSC sacrificial-microgel scaffold combines growth-factor-containing PRP with cells present from implantation, with rat repair/reproductive observations and a two-macaque exploratory comparison [117]. Sections 4.2–4.3 examine its coupled pore-generation/release behavior and the limits of a sequence-specific interpretation.

3.6 Recovering hormone responsiveness and reproductive function

A regenerated cavity may remain functionally incomplete even after collagen decreases and thickness rises. Hormone-responsive stroma, a receptive epithelium and glandular–vascular support must operate together. Local estradiol thermogels, aloe/poloxamer matrices and PLGA depots attempt to control exposure, whereas protein- and growth-factor-bearing scaffolds seek to restore supporting cell states [118–123]. The available characterization does not establish a causal micellar-size effect for a bulk thermosensitive estradiol gel; it is more accurately treated as a local depot [118].

New human-cell studies make the mechanics-to-function link more concrete. On NorHA gels with measured compressive moduli of 5.1 ± 0.187 and 15.8 ± 1.57 kPa, hormone treatment increased stromal-cell nascent ECM deposition by approximately 25% and 11%, respectively, with similar deposition after treatment [31]. Its prolactin assay was performed on glass and should not be assigned separately to either gel. In a different uterine-fibroblast model, nominal 100-kPa substrates attenuated early decidual responses relative to 4-kPa substrates, while ligand identity modified progesterone-associated signaling [32]. This endometriosis-adjacent study examines a different experimental system, with differences in chemistry, hormone regimen and stiffness range that limit direct comparison with IUA scaffold studies. In Ishikawa epithelium, 4- versus 23-kPa substrates produced mean traction stresses of 92.09 ± 21.11 versus 248.15 ± 109.90 Pa without a significant change in apical cellular elastic modulus [33]. Trophoblast-spheroid adhesion in this assay is not embryo implantation. Together, these findings favor testing hormone responsiveness on a candidate matrix, but define neither a universal optimal modulus nor clinical reproductive efficacy.

Defined epithelial–stromal co-cultures and decidual assembloids provide complementary functional assays [34, 35]. In the assembloid study, dasatinib-pretreated constructs were structurally persistent but failed to support expansion of five co-cultured human blastocysts, unlike untreated constructs [35]. Embryos were placed into matrix pockets, bypassing luminal attachment; the experiment therefore probes embryo–stromal interactions rather than physiological implantation. It illustrates why structural persistence and secretory-marker induction need not imply reproductive permissiveness. Such models can interrogate function before transplantation, but cannot substitute for pregnancy, placentation and offspring follow-up or establish that a material treats IUA.

Human cell–scaffold studies provide the strongest available reproductive anchor. Phase-I and before–after studies established feasibility in recurrent IUA or refractory thin endometrium, but concurrent surgery and hormonal management limit attribution [124, 125]. In the small randomized hUC-MSC/collagen trial, live births occurred in 3/11 treated women versus 1/13 controls; the risk ratio was 3.55 with a 95% confidence interval of 0.43–29.42 [7]. A larger trial randomized 152 women and reported per-protocol ongoing pregnancy in 45/72 versus 28/68 and live birth in 41/72 versus 26/68 for bone-marrow-cell scaffold plus Foley catheter versus Foley control; the reported per-protocol live-birth risk ratio was 1.49 (95% CI 1.04–2.14; P=0.027) [6]. These results support evaluation of the complete treatment strategy, not a nano-specific benefit or an isolated scaffold effect. The placental observations are addressed separately in Section 5.2.

Table 2 retains these human denominators alongside animal timing, controls and release observations. It is intended to show what each experiment establishes, not to rank dissimilar products using cross-study percentages. Most new material studies intervene around an acute injury. Their gestational or histological improvement should therefore be described as prevention or early regeneration unless established adhesions and a delayed treatment interval were demonstrated.

Just Accepted

Table 2. Observed study-level evidence for representative biomaterial interventions: clinical comparators and experimental injury models

Study / indication and timing	Actual comparison	Delivery / residence measurement	Functional / reproductive observation	Interpretation limit
In-situ barrier RCT [46]; 150 women after adhesiolysis or myomectomy.	Hydrogel 99; no barrier 51; blinded second-look assessment at 8 weeks.	Patient-level residence unmeasured; proposed 2–3 weeks is not clinical pharmacokinetics.	Higher adhesion-free status in adhesiolysis subgroup; fertility unassessed.	Anatomical barrier benefit, not nano-specific benefit; mixed procedures and subgroup precision limit inference.
Bone-marrow-cell scaffold RCT [6]; 152 randomized after adhesiolysis.	Cell–scaffold plus Foley versus Foley; per-protocol 72 versus 68.	No quantitative clinical product-residence or release curve.	Ongoing pregnancy 45/72 versus 28/68; live birth 41/72 versus 26/68; reported per-protocol live-birth RR 1.49 (95% CI 1.04–2.14; P=0.027).	Complete-strategy comparison, not isolated scaffold effect. Obstetric and center-exclusion denominators differ; see Section 5.2.
hUC-MSC/collagen RCT [7]; refractory thin endometrium; post-adhesiolysis/plowing implantation.	Cell-loaded versus saline-loaded scaffold; 25 randomized, 24 treated/analyzed (11/13).	No quantitative patient-level cell/scaffold residence curve.	Live birth 3/11 versus 1/13; RR 3.55 (95% CI 0.43–29.42); urticaria 2/11.	Added-cell comparison; imprecise, nonsignificant reproductive estimate.
Ru-SAN@CH [10]; atomically dispersed Ru/carbon in chitosan gel; immediate unilateral mouse ethanol injury treatment.	Sham, injury, CH, free Ru-SAN, Ru-SAN@CH.	~70% gel degradation at 10 days in vitro; not uterine Ru exposure.	Mean live-born litter size ~8.8 versus 4.3 with injury; eight mice/group in offspring cohort.	Component comparison; size/atomic-dispersion causality unresolved. Intact contralateral horn limits whole-litter attribution; counts are not live-birth probabilities.
QOHP/siSMAD3 [75]; G5 PAMAM/siRNA in modified hyaluronate; immediate rat scraping-injury treatment.	Sham, injury, empty QOHP, siRNA alone, QOHP@siRNA.	Main text reports uterine gel persistence 3–5 days; in-vitro cellular uptake/silencing through day 5 is not release kinetics.	More embryos and offspring-weight observations reported.	Polyplex size unreported in main text; carrier evidence, not demonstrated nanoscale superiority. Reproductive timing/cohort allocation unresolved.
ADMSC–SF/PCL mats [84]; electrospun fibers implanted seven days after rat scraping/LPS injury.	Control, sham, injury, E2+mat, E2+cell–mat, cell–mat; E2 intramuscular.	Sutured placement; no quantitative uterine cell/material residence or drug-release curve.	Improved thickness, glands and vascular/decidualization-associated markers; no mating experiment in main text.	No free-cell-only, unmedicated cell-free mat or matched nonfibrous animal arm. Hormone/cell/scaffold contributions incompletely separated; fiber-size causality unresolved.
TSG6-EV thermogel [12]; acute murine injury; day-14 repair assessment.	Empty CS/GP, control-vector EV gel, TSG6-EV gel; separate free/gel EV tracking.	2% CS/GP nearly degraded by day 9 in lysozyme; fluorescent EV tracking through day 7.	Improved fibrosis, thickness, glands, CK18/CD31 and ER-associated measures; no reproductive experiment in main text.	Engineered cargo and retention supported; independent EV-size contribution unresolved.
Hollow MnO_2 gel [11]; early uterine injury treatment.	Composite HME, natural repair and material-component arms.	E2 release measured through ~9 days in PBS/0.1% Tween 80 in vitro. Main text reports complete gel degradation at 30 days with hyaluronidase and no detectable in-vivo gel residue at 45 days.	HME200 ABTS scavenging 86.5% in vitro. Injured-right-horn pregnancy at gestational day 16: 45.5% versus 9.1% natural repair; 11 females in each of these two groups; no live-birth endpoint.	Formulation effect, not isolated size/catalysis contribution. Degradation/residue observations are main-text reports of supplementary findings; gel disappearance does not resolve nanozyme exposure or metal fate.
Decidualized ECM/Tβ4–PLGA [78]; immediate mouse mechanical/ethanol injury treatment.	Sham, injury, microspheres, conventional/decidualized ECM and respective composites.	35.6-μm microspheres; ~70% Tβ4 release by day 3 alone; composite release extended over the ten-day in-vitro assay.	Day-14 repair and reproductive observations; six animals/cohort.	Sustained single-cargo delivery, not isolated sequence benefit. Gestational-day-19 collection and offspring descriptions require reconciliation.
PRP/ADSC microgels [117]; immediate rat injury treatment; macaque feasibility, one animal/condition.	Empty scaffold, free PRP, free ADSCs, composite; no matched simultaneous combination.	BSA proxy plateau ~48 h; VEGF/EGF release >48 h; gelatin dissolution creates pores.	Rat repair and gestational embryos; fertility cohort five females/group, but three embryo-count observations/group.	Subset relation unresolved; no macaque fertility test. Combination/differential presentation, not proven timing superiority.
CeTA@GPP [71]; 100 μL gel at rat scraping/LPS injury surgery.	Sham, injury, GPP, CeTA@GPP; separate CeTA/CeO_2 /TA assays.	Day-8 TA release 96.87% in H_2 O_2 versus 53.67% PBS; label tracked to day 14.	Three females/group; mean mid-gestation embryos 14.7 composite, 11.7 GPP, 6 injury, 13.7 sham.	No demonstrated fertility superiority over GPP or live birth. Released TA/label does not measure active intact nanozyme.

Just Accepted

Study / indication and timing	Actual comparison	Delivery / residence measurement	Functional / reproductive observation	Interpretation limit
Iron-trapping BPC [72]; rat right-horn scraping/ethanol injury; index surgery.	Sham, saline, PLA film, BPC; additional PA-free gel comparison.	Oxidant-enhanced PA release; figure/method time scales differ. Day-28 near-disappearance measured subcutaneously.	Day-3 redox/day-14 repair; reported injured-side pregnancy 83% versus 33%, denominator unresolved.	Not a nanozyme; PA removal alters network chemistry. Nonuterine degradation and unresolved fertility denominator limit interpretation; no live birth.
Responsive antifouling DRH [62]; intraoperative rat mechanical-injury treatment.	Injured vehicle versus DRH; paired healthy left horns; three females/group.	In-vitro degradation by day 13; uterine fluorescence through day 7; no delivered drug.	Relative embryo number improved after mating from postoperative day 14; no live-birth endpoint.	Vehicle control does not isolate antifouling, barrier, ROS consumption or degradation contributions; absolute embryo counts unresolved.
VEGF/IGF-1 depot [82]; immediate photocured mouse mechanical-injury treatment.	Sham, injury, blank gel, single factors, simultaneous G-VI, sequential G-V-I.	VEGF >60% within four days; IGF-1 shifted later, through day 16 in vitro.	Day-14 thickness 243.49±30.89 versus 178.66±20.86 μm; fibrosis 13.3±2.4 versus 21.8±2.3%. Gestational-day-16 embryos 9±1 versus 6±2 (SD); six females/endpoint; higher live-born pup counts in separate delivery cohort; pup weights followed to day 12.	Retained-dose equivalence and active exposure unresolved; compartmentalization differs. Sham-referenced count indices are not per-female probabilities; short-term follow-up is not comprehensive safety (Section 4.3).
Printed porous scaffold [83]; rat scraping/LPS injury; treatment one week later.	Blank PH, free ADSCs/exosomes, ADSC@PH, Exo@PH, sham/injury.	Porogen increased pores ~5.3 to 19.2 μm; needle passage/compression measured; no uterine cargo-release curve.	Histological/glandular and fibrosis-associated repair; no fertility experiment in main text.	No cell-matched nonporous animal arm; porosity-specific benefit unresolved.
Janus bioadhesive [55]; immediate rat scraping-injury placement.	Sham, saline injury, Interceed, Janus material; separate abdominal experiments.	Wet-skin lap shear ~98 kPa, peel toughness 325 J/m²; ~two-week persistence measured subcutaneously.	Uterine repair and gestational/newborn observations.	No isolated nanofiber benefit or measured uterine residence window; horn/embryo counting does not establish precise live-birth probability.
Vericiguat depot [77]; rat scraping; treatment after three estrous cycles (~12 days).	Sham, injury, oral drug, local free drug (2 mg), empty gel, loaded gel (2 mg).	~15% drug release by day 3 in PBS/0.3% SDS; ~20% uterine gel mass at day 15.	Repair after four treatment cycles; fetal outcomes, five females/group; no live-birth endpoint.	Nominal local dose matching; oral route differs. Carrier mass is not drug kinetics; printed fetal-count formula and reported indices differ.

Selection: this purposive, non-exhaustive comparison includes directly relevant clinical or uterine-injury studies with identifiable controls and measured outcomes, chosen to represent clinical benchmarks, characterized nano-features, or informative carrier/scaffold and timing comparisons. It is not a platform ranking, consensus or minimum dataset; structural nanoscale classification is distinguished from demonstrated functional attribution. Outcomes and counting units are not interchangeable. Unless stated otherwise, animal treatment concerns acute injury/early repair, not proven chronic-scar reversal. Source locators (primary reports): [46] Methods/Results; [6] main Tables 2–4 and supplement Tables 1–3; [7] Methods/Results; [10] Fig. 3 and Section 4.10; [75] Figs. 6–7,11; [84] Sections 2.5–2.6 and Figs. 2–4; [12] Figs. 6–7 (PDF pp. 9–11); [11] Figs. 2J,L and 5, Sections 3.3/3.5; [78] Figs. 4k,7 and fertility Methods; [117] Figs. 3I–K,6 and Methods (pp. 15–16); [71] Figs. 3K,8; [72] Figs. 1k,6–7; [62] Fig. 8G–H and Section 2.11; [82] Methods and Figs. 3,5,7 (PDF pp. 5–6,9–15); [83] characterization/animal Methods (pp. 3–9); [55] interface/fertility experiments; [77] release/retention/fertility experiments. CH, chitosan hydrogel; QOHP, quaternized oxidized hyaluronate/PAMAM hydrogel; PAMAM, polyamidoamine; SF/PCL, silk fibroin/polycaprolactone; E2, estradiol; LPS, lipopolysaccharide; EV, extracellular vesicle; CS/GP, chitosan/β-glycerophosphate; ECM, extracellular matrix; PRP, platelet-rich plasma; ADSC/ADMSC, adipose-derived stem/mesenchymal stem cell; CeTA, cerium–tannic-acid complex; GPP, gelatin-PBA/PVA; BPC, borax–protocatechuic aldehyde–chitosan; PA, protocatechuic aldehyde; PLA, polylactic acid; RR, risk ratio; CI, confidence interval.

4. Cross-platform structure–property–function relationships and minimum sufficient material complexity

Platform names do not predict intrauterine behavior. The useful comparison is whether a controllable parameter changes coverage, retention, transport, cell interaction or local exposure, and whether that change improves the intended outcome. The following synthesis separates experimentally observed links from design inferences. We propose minimum sufficient material complexity as a qualitative comparison principle; its use for clinical scoring, treatment selection or therapeutic ranking remains unvalidated.

4.1 Geometry, surface chemistry and interfacial behavior

Asymmetric interfaces resolve the competing demands of fixation and anti-adhesion by assigning them to different surfaces. Arrowhead patches, EV-loaded Janus microneedles and microstructured bioadhesives demonstrate implementations of this spatial division [13, 53, 55]. Their common advantage is directional contact, not an inherent temporal sequence. Compared with an injectable gel, a prefabricated interface can offer more defined orientation but requires correct placement and complete coverage of an irregular lesion; a strong planar adhesion test does not establish those behaviors in a uterine cavity.

Surface chemistry also changes cell recognition. Synthetic endometrial matrices use defined adhesive and ECM-binding motifs to support organoid growth and epithelial–stromal co-culture [34, 97]. In the endometrial extension of a primarily intestinal-organoid study, day-8 median organoid diameters were 85 μm with GFOGER, 58 μm with PHSRN-K-RGD and 91 μm in Matrigel [97]. These growth and polarity observations do not demonstrate hormone responsiveness or an isolated mechanical effect. In an adjacent scaffold-design study,

Under Peer Review

galactose-functionalized electrospun PCL fibers supported human uterine fibroblast culture; animal testing was confined to dorsal subcutaneous implantation [126]. Surface modification and alignment also changed wettability, fiber diameter, porosity and tensile properties. Neither cell compatibility nor subcutaneous histology establishes endometrial regeneration or an isolated nanoscale advantage.

Hydrated antifouling domains reduce unwanted adsorption [37, 51, 62], whereas catechol-containing formulations favor tissue attachment [63]. The trade-off is functional: excessive antifouling may impair desired integration on the tissue-facing side, and excessive bilateral adhesion may obstruct separation. Janus geometry can partition these functions, but adds an orientation requirement; an injectable composite trades directional precision for cavity conformity. Which compromise is useful depends on the lesion and delivery route.

4.2 Network architecture, mechanics and transport

Increasing polymer concentration or crosslinking commonly changes mechanics, mesh size, swelling, diffusion and degradation together. Consequently, a more durable gel may retain cargo but restrict cell spreading or slow clearance; a more open construct may support transport while losing mechanical integrity. Microfluidically templated scaffolds and injectable printed porous constructs demonstrate controllable architectures, yet their regenerative comparisons also involve drug or cell loading [52, 83]. Structural tunability alone does not identify an optimum pore diameter.

Sacrificial microgels provide a concrete coupled example [117]. Gelatin dissolution at physiological temperature created pores in a printed GelMA scaffold, increased swelling and degradation relative to the nonsacrificial matrix, and changed compressive behavior. The same event also altered PRP-associated release and the environment of retained ADSCs. Thus better cell support cannot be attributed solely to porosity, nor can pore generation alone establish that sequential therapy caused the reproductive effect. Adhesive HMD formulations similarly vary interface chemistry, network properties and cell support together [63].

Elastic stiffness and time-dependent relaxation are distinct variables. In a nonuterine stem-cell study, hydrogels with tunable stress relaxation showed different spreading and differentiation despite similar initial modulus and nominal ligand density within each comparison [127]. This is a transferable experimental principle, not an IUA therapeutic prescription. A synthetic PEG endometrial co-culture model spanning rheology-derived Young's moduli of approximately 0.3–6 kPa supported stromal prolactin responses across the tested formulations and hormone-dependent epithelial–stromal behavior over 15 days [34]. Polymer content and ligand accessibility co-varied, so these data do not select one universal optimum. The hormone/ECM studies [31, 32] and organoid-matrix comparisons [97] likewise show why growth, differentiation and remodeling must be assessed separately. A matrix can be permissive for one cell state but inappropriate for another.

Reported storage modulus, compressive modulus and indentation-derived Young's modulus should not be pooled as equivalent values. Nor should a cell-culture stiffness window be transferred directly to a swelling, degrading intrauterine implant. For IUA, the unresolved relationship is how evolving matrix mechanics alter stromal activation, endothelial survival and hormonal function in the same construct. The Piezo1 findings provide a biological reason to measure that relationship; they do not show that any existing gel achieves a clinically validated mechanical target [24].

4.3 Residence, release and temporal coordination

Residence of a carrier, release of a label, intact-cargo exposure and matrix degradation are different measurements. The TSG6-EV study separately measured gel degradation and fluorescent EV retention [12]; the EV-loaded Janus patch reported approximately 80% vesicle release over seven days [13]. These assays are useful, but fluorescent persistence does not identify the concentration of intact, active EVs. Likewise, a protein-release curve does not establish its retained potency or tissue-level exposure. Thiol-rich networks illustrate how reactive chemistry, tissue retention and repair can be combined (Figure 9) without establishing a sequence of independently released therapies [73].

The vericiguat depot illustrates the measurement distinction directly: approximately 15% drug release by day 3 was measured in PBS containing 0.3% SDS, whereas about 20% gel mass remained intrauterine at day 15 [77]. The former measures drug transport under the assay conditions and the latter carrier persistence; neither determines the concentration or activity of vericiguat in the repairing endometrium.

Just Accepted

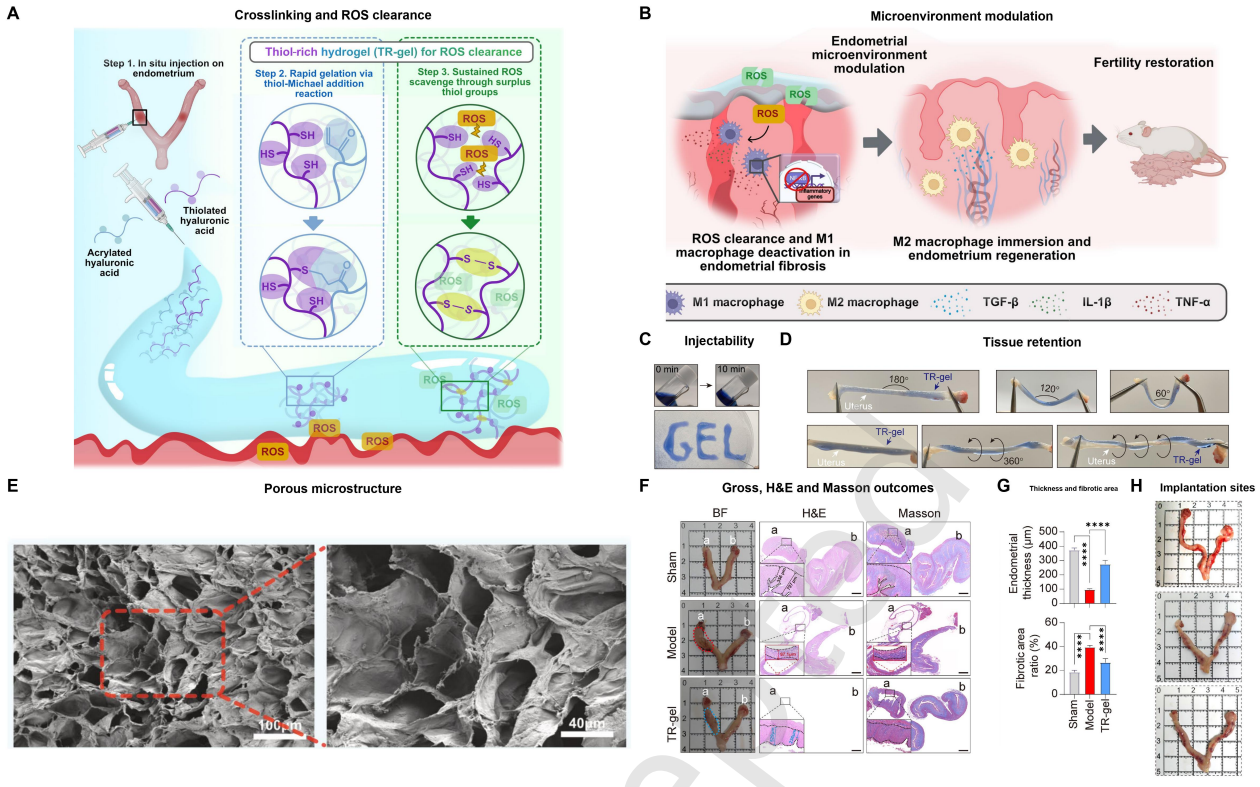


Figure 9. Thiol-rich immunomodulatory injectable hydrogel for endometrial repair. (A,B) Thiol-Michael crosslinking, ROS clearance and microenvironment modulation; (C–E) injectability, tissue retention and porous microstructure; and (F–H) gross and histological outcomes, endometrial thickness, fibrotic area and implantation sites. With permission under CC BY 4.0. [73]

Spatial asymmetry, stimulus response and sequential delivery answer different questions. Janus surfaces determine where an interaction occurs [55]. ROS- or pH-sensitive bonds determine under which chemical conditions a network changes [62, 71, 72]. Sequential delivery additionally requires evidence for the relative timing of two activities. A response observed in peroxide-containing buffer supports chemical sensitivity; it does not demonstrate that the material detects a particular repair phase in vivo.

The VEGF/IGF-1 system includes directly co-loaded simultaneous and microsphere-in-gel sequential formulations [82]. The comparison does not establish equivalence of retained doses, and growth-factor compartmentalization and binding differ; it therefore tests complete delivery formulations, not release order alone. Untreated-injury time courses showed overlapping early Vegfa and later Igf1 expression. More than 60% of VEGF was released within four days in vitro, whereas IGF-1 release shifted later and persisted through day 16. This provides a biological timing rationale, not strictly nonoverlapping release or a validated universal schedule.

Within these limits, day-14 thickness was 243.49 ± 30.89 versus 178.66 ± 20.86 μm and fibrosis area was 13.3 ± 2.4% versus 21.8 ± 2.3% for sequential versus simultaneous delivery (mean ± SD; six mice/group) [82]. The original study reports $P<0.001$ for thickness and $P<0.01$ for fibrosis in its pairwise figure annotations and specifies one-way ANOVA in its methods. Exact P values, test statistics and the post-hoc/multiplicity procedure are not specified in the available main text. The findings favor the tested sequential formulation for these repair endpoints, but local active-factor pharmacokinetics and serial treated-tissue transitions were not jointly demonstrated.

Reproductive testing started after 14 treatment days, with 12 females/group: six examined at gestational day 16 and six followed through delivery [82]. Sequential versus simultaneous delivery yielded mean embryo counts of 9 ± 1 versus 6 ± 2 (SD); source Fig. 7c reports $P<0.01$, and Fig. 7g reports higher live-born pup counts with sequential delivery ($P<0.001$). Pup weights were followed through postnatal day 12. These are count-based outcomes; the source's sham-referenced implantation/live-birth indices are not per-female pregnancy or live-birth probabilities. Short-term pup-weight follow-up does not establish comprehensive reproductive safety, and the formulation differences still prevent isolating release order.

Two existing examples support narrower timing claims. In the PRP/ADSC sacrificial-microgel scaffold, the model-protein curve approached a plateau at 48 h and VEGF/EGF release was measured over more than 48 h; cells were present in the construct from implantation [117]. The animal groups included empty scaffold, free PRP, free ADSCs and the complete product, but not a dose-matched simultaneous PRP-plus-ADSC delivery construct with the same architecture. This supports differential presentation and a combination effect, not isolated superiority of release order. Reproductive sampling was incompletely reconciled: five females per group were specified for pregnancy assessment, whereas the embryo-count figure showed three observations. The macaque comparison used one animal per condition. The ECM/Tβ4 system instead demonstrates ten-day sustained release of a single cargo from microspheres in an active matrix [78], a different delivery mechanism from sequential dual-cargo therapy.

Taken together, the studies justify testing temporal coordination, but do not establish a universal stage-matched schedule. A proposed discriminating experiment would relate local active-

cargo exposure to serial repair-state measurements and compare alternative schedules while keeping dose, material composition and relevant mechanics comparable.

4.4 What is specifically enabled by nanoscale engineering?

Here, intrinsically nanoscale describes the active entity itself, such as a characterized nanoparticle, catalytic nanostructure or nanoscale EV population. Nano-enabled describes a bulk construct containing such entities or a designed nanoscale architecture, including nanofibrous mats; both terms describe structure before therapeutic advantage is assessed. Candidate functions that may depend on these features include catalysis, intracellular delivery, tissue interaction, molecular transport, controlled release and ECM-scale cell regulation. Each requires a specific feature–function test, because the same broad function may also be achievable with a simpler material. Conventional films, ECM gels and micrometer-scale depots therefore remain informative benchmarks [4, 5, 78].

We assess four questions in sequence: is the proposed nanoscale feature characterized; does its component contribute to a measured function; do feature-matched controls establish dependence on that feature; and does the complete product improve an indication-relevant simpler comparator? Empty-versus-loaded and free-versus-carrier-bound cargo comparisons address component and delivery contributions. A feature-deficient or architecture-matched analogue with comparable composition, dose and exposure addresses the third question; a relevant simple barrier or depot addresses the fourth. Ru single-atom, MnO_2 and cerium–tannic-acid systems provide catalytic characterization, but their animal efficacy comparisons do not fully isolate nanoscale size from chemistry, loading and retention [10, 11, 71]. Missing feature-matched controls leave that attribution unresolved.

For EVs, biological cargo activity and carrier-mediated retention are more directly supported than an independent size advantage [12, 13, 64]. Cell-bearing SF/PCL mats and chorionic-villus-derived ECM networks connect scaffold design with cell support or EV production, but their comparisons vary scaffold composition, cell loading or the 3D culture environment rather than independently testing nanoscale fiber dimensions [84, 128]. The adjacent galactose/PCL study demonstrates the same attribution problem for surface-functionalized fibers [126]. A micro–nano cell/pirfenidone construct adds delivery possibilities, yet its component comparisons do not alone establish superiority to a simpler non-nano depot at equivalent exposure [79]. The key experimental question is which function requires a nanoscale feature and whether that contribution can be separated from the rest of the construct.

4.5 When is additional material complexity justified?

Minimum sufficient material complexity begins with the unmet function. If inadequate coverage causes failure, changing geometry or gelation may be more relevant than adding a drug. If coverage is adequate but local activity is short-lived, a depot may be justified by measured exposure. If a depot still cannot achieve intracellular delivery or catalytic control, a defined nanocomponent may add value. If epithelial–stromal or vascular coordination remains deficient, a multicellular or ECM-based construct may be justified by functional evidence. These are alternative problem-specific decisions, not a hierarchy in which more components imply better therapy.

The existing comparisons support different parts of that reasoning. The Tβ4 microsphere/ECM release experiment demonstrates a transport benefit of adding a matrix [78]. Janus systems demonstrate spatial division of conflicting interface functions [13, 55]. The hUC-MSC trial compares a cell-loaded scaffold with a saline-loaded scaffold but remains statistically imprecise [7]; the larger bone-marrow-cell trial tests a combined strategy against Foley control and therefore cannot isolate the scaffold contribution [6]. Organoid and vascularized constructs enable tissue interactions that acellular barriers cannot provide, but bring donor, multicellular composition and matrix-definition burdens [98, 99].

The appropriate conclusion is consequently product- and indication-specific. Added complexity is supported when the additional function is measured, a relevant simpler comparison fails to provide it, and the biological gain survives that comparison. Where only composite-versus-injury efficacy exists, the construct remains promising but its complexity is not yet experimentally justified. This principle also prevents comparing pregnancy percentages from different species, injury depths or analysis populations as if they were a head-to-head materials ranking.

5. Unresolved translational barriers

5.1 Indication, model and outcome alignment

Promising formulations face a central translational obstacle: acute experimental repair models differ from the clinical settings in which treatment is needed. Immediate dosing after scraping or chemical injury generally evaluates prevention or early regeneration. Recurrence prevention requires an established adhesion followed by adhesiolysis; reversal of chronic fibrosis requires delayed treatment after the lesion has been documented. Full-thickness reconstruction and hormone-responsive organoid culture address additional biological questions but cannot supply direct evidence for either indication. The small primate studies extend feasibility while leaving efficacy and reproductive follow-up uncertain [109, 117].

Study interpretation also depends on the unit of analysis. Female animals are the units for pregnancy and litter outcomes, with horns and embryos nested within them. In clinical work, outcomes among all randomized women, per-protocol participants and those who reach embryo transfer should remain distinct [6, 7, 45]. Thickness, fibrosis area and vessel markers are useful intermediate measures, but neither their normalization nor increased implantation counts establish cyclic function, live birth or long-term offspring health.

5.2 Product fate and reproductive safety

Local administration does not establish local confinement or clearance before conception. Catalysts raise questions about elemental speciation and ovarian/systemic exposure; degradable networks about reactive residues and fragments; EV/cell constructs about active biological persistence. Label loss alone cannot resolve these questions. Tracking must identify what the signal represents before it is used to time conception or infer absence of an active product.

The larger bone-marrow-cell scaffold trial used 72 versus 68 participants for per-protocol efficacy, but its main obstetric table reported placenta accreta as 9/72 versus 2/70 [6]. The control denominator of 70 is numerically consistent with 73 full-analysis-set participants minus three lost to follow-up; the exact outcome-specific population is not explicitly defined. The supplement reports placental adhesion as 9/68 versus 2/68 in a separate analysis excluding the second center, not a correction of the main table. These are source-specific exploratory

Just Accepted

observations with different analysis populations, not a pooled effect or proof that the intervention caused placental disease. They nevertheless show why pregnancy benefit and placental outcomes need joint assessment. The smaller hUC-MSC study also reported urticaria in 2/11 treated participants and was too small to resolve uncommon or delayed risks [7]. Animal embryo counts or short-term maternal-organ histology cannot close these gaps.

Formal safety frameworks are distinct from the authors' design suggestions. ISO 10993-1:2025 addresses device biological safety within risk management, ISO 10993-3:2026 addresses relevant genetic, carcinogenic and reproductive/developmental endpoints for devices, and ICH S5(R3) covers reproductive and developmental toxicity for pharmaceuticals [129–131]. Their applicability depends on product composition and regulatory context; the present narrative synthesis does not establish a universal IUA testing checklist or clearance threshold.

5.3 Manufacturing and reproducible product identity

The unresolved manufacturing question is whether the measured research function survives scale-up, storage, sterilization and deployment. For a hydrogel, this includes the coupled behavior of gelation, adhesion and degradation. A catalytic composite additionally depends on reproducible active sites and dispersion. ECM products inherit tissue-source and processing variation [132], while EV formulations require identity, impurities, dose and post-release potency to be controlled [108]. Cell constructs add viability and function after loading and transport. These variables belong to the administered combination, not merely to separately characterized starting components. Demonstrating an effect from one laboratory batch therefore remains different from establishing a reproducible clinical product.

6. Priorities and future perspectives

The following three priorities are the authors' research recommendations derived from this narrative comparison. First, temporal designs should be tested against alternative schedules using the same model, matched dose and serial measurements of active exposure and repair. The current release data support this experiment but do not predetermine the optimal sequence.

Second, added components should be evaluated against the specific simpler solution they are meant to improve. Targeted or engineered EVs and transient nucleic-acid systems offer ways to perturb profibrotic signaling [75, 133, 134], but their value depends on target engagement, reversibility and an increment over a less complex delivery strategy. Cell-free and multicellular constructs should likewise be compared by retained biological function rather than by the number of incorporated modules.

Third, functional recovery should be connected to product fate and subsequent reproduction. Hormone-responsive co-cultures and assembloids can test coordinated tissue behavior, while longitudinal animal and clinical follow-up addresses implantation, placentation and live birth. Material-enabled monitoring has a focused role here: calibrated signals for cavity coverage, displacement, degradation or clearance could inform removal, redosing or conception timing. Such monitoring remains a prospective tool, not an established clinical IUA nanodiagnostic platform.

7. Conclusion

IUA biomaterial design is most coherently organized around six overlapping repair requirements: separation and epithelial continuity, resolution of maladaptive immune–stromal signaling, control of oxidative injury, limitation of fibrotic remodeling, reconstruction of tissue niches, and recovery of hormone-responsive reproductive function. This framework connects mechanism to a material parameter, an observed local behavior and an appropriately bounded outcome.

Human evidence is most developed for relatively simple barriers and selected cell–scaffold strategies. Nanoscale catalysts, EV composites, responsive depots and sequential constructs offer experimentally useful functions, but their specific contribution is often incompletely separated from chemistry, physical separation or total exposure. Spatial asymmetry and sustained or triggered release should not be presented as proof of stage-matched treatment. The most defensible development path is to establish the additional function that a component provides, demonstrate its value within the intended indication, and connect recovery to product fate and reproductive outcomes. Minimum sufficient material complexity focuses these comparisons on the additional function provided by each component.

Data availability

Not applicable.

Acknowledgements

This work was supported by grants from the Jilin Province Department of Finance (No. J1SRCZX2025-088) and the National Natural Science Foundation of China (82403881).

Declaration of competing interest

All the contributing authors report no conflict of interests in this work.

Author contribution statement

J. Tian: Writing – review & editing, Writing – original draft; H. Zhou: Writing – review & editing, Writing – original draft; M. Zhou: Writing – review & editing, Writing – original draft; Y. Pan: Writing – review & editing, Writing – original draft.

Informed consent

Not applicable.

Ethics statement

Not applicable.

Use of AI statement

During the preparation and revision of this manuscript, the authors used ChatGPT and Codex to assist with language editing, literature extraction, organization and drafting. The authors are responsible for checking the original sources, reviewing and editing the content, and taking full responsibility for the publication.

Table of Contents summary

This critical narrative review links six overlapping repair requirements in intrauterine adhesions to material structure, local behavior and functional endometrial recovery. It compares observed timing, controls and reproductive outcomes to distinguish nanoscale structure from demonstrated nano-specific benefit and to identify when additional material complexity is justified.

References

[1] Yao, S.; Zhou, Z.; Wang, L.; Lv, H.; Liu, D.; Zhu, Q.; et al. Targeting endometrial inflammation in intrauterine adhesion ameliorates

Just Accepted

endometrial fibrosis by priming MSCs to secrete C1INH. *iScience* **2023**, *26*, 107201. https://doi.org/10.1016/j.isci.2023.107201.

[2] Lv, H.; Sun, H.; Wang, L.; Yao, S.; Liu, D.; Zhang, X.; et al. Targeting CD301+ macrophages inhibits endometrial fibrosis and improves pregnancy outcome. *EMBO Mol. Med.* **2023**, *15*, e17601. https://doi.org/10.15252/emmm.202317601.

[3] Li, Y.; Wu, W.; Lv, H.; Shi, L.; Wang, Z.; Zhu, C.; et al. Single cell multiomics revealed fibrotic trajectories of endometrial cells and interaction with the pro-fibrotic macrophages in intrauterine adhesion. *Genome Med.* **2026**, *18*, 68. https://doi.org/10.1186/s13073-026-01641-x.

[4] Wang, H.; Gu, X.; Li, T.; Niu, X.; Zhang, H.; Yang, Q.; et al. Effect of collagen scaffold vs. intrauterine device on preventing recurrence of intrauterine adhesions: a multicenter randomized controlled trial. *Fertil. Steril.* **2026**, *125*, 708–716. https://doi.org/10.1016/j.fertnstert.2025.08.035.

[5] Weyers, S.; Capmas, P.; Huberlant, S.; Dijkstra, J. R.; Hooker, A. B.; Hamerlynck, T.; et al. Safety and Efficacy of a Novel Barrier Film to Prevent Intrauterine Adhesion Formation after Hysteroscopic Myomectomy: The PREG1 Clinical Trial. *J. Minim. Invasive. Gynecol.* **2022**, *29*, 151–157. https://doi.org/10.1016/j.jmig.2021.07.017.

[6] Zhu, H.; Li, T.; Xu, P.; Ding, L.; Zhu, X.; Wang, B.; et al. Effect of autologous bone marrow stem cells-scaffold transplantation on the ongoing pregnancy rate in intrauterine adhesion women: a randomized, controlled trial. *Sci. China Life Sci.* **2024**, *67*, 113–121. https://doi.org/10.1007/s11427-023-2403-7.

[7] Hou, Z.; Yang, T.; Xu, D.; Fu, J.; Tang, H.; Zhao, J.; et al. hUC-MSCs loaded collagen scaffold for refractory thin endometrium caused by Asherman syndrome: a double-blind randomized controlled trial. *Stem Cells Transl. Med.* **2025**, *14*, szaf011. https://doi.org/10.1093/stcltm/szaf011.

[8] Zhu, Q.; Yao, S.; Ye, Z.; Jiang, P.; Wang, H.; Zhang, X.; et al. Ferroptosis contributes to endometrial fibrosis in intrauterine adhesions. *Free Radic. Biol. Med.* **2023**, *205*, 151–162. https://doi.org/10.1016/j.freeradbiomed.2023.06.001.

[9] Li, Y.; Zhao, H.; Chen, X.; Zhang, J.; Du, Q.; Shen, Y.; et al. Spatial and temporal single cell multi-omics in mice reveals macrophage-SFRP4+ stroma interactions promoting endometrial regeneration via TNF-α. *Cell Rep.* **2026**, *45*, 117434. https://doi.org/10.1016/j.celrep.2026.117434.

[10] Liang, Y.; Meng, J.; Yu, Z.; Guo, Y.; Zhang, X.; Yan, Y.; et al. Ru single-atom nanozymes targeting ROS-ferroptosis pathways for enhanced endometrial regeneration in intrauterine adhesion therapy. *Biomaterials* **2025**, *315*, 122923. https://doi.org/10.1016/j.biomaterials.2024.122923.

[11] Xu, Y.; Ye, Z.; Hu, S.; Chu, L.; Xin, L.; He, W.; et al. A hollow MnO(2) nanozymes empowered injectable hydrogel for intrauterine adhesion therapy by alleviating oxidative stress and promoting endometrial repair. *Biomater. Sci.* **2026**, *14*, 2361–2371. https://doi.org/10.1039/d6bm00109b.

[12] Sun, H.; Dong, J.; Fu, Z.; Lu, X.; Chen, X.; Lei, H.; et al. TSG6-Exo@CS/GP Attenuates Endometrium Fibrosis by Inhibiting Macrophage Activation in a Murine IUA Model. *Adv. Mater.* **2024**, *36*, e2308921. https://doi.org/10.1002/adma.202308921.

[13] Wang, H.; Chen, W.; Liu, Y.; Zhu, Y.; Huang, Y.; Lu, Z. Janus adhesive microneedle patch loaded with exosomes for intrauterine adhesion treatment. *J. Mater. Chem. B* **2024**, *12*, 3543–3555. https://doi.org/10.1039/d3tb03036a.

[14] Qin, Z.; Yu, Q.; Long, Y. Unveiling the Pathological Landscape of Intrauterine Adhesion: Mechanistic Insights and Exosome-Biomaterial Therapeutic Innovations. *Int. J. Nanomedicine* **2025**, *20*, 9667–9694. https://doi.org/10.2147/ijn.s527637.

[15] Liu, Y.; Jia, D.; Li, L.; Wang, M. Advances in nanomedicine and biomaterials for endometrial regeneration: a comprehensive review. *Int. J. Nanomedicine* **2024**, *19*, 8285–8308. https://doi.org/10.2147/IJN.S473259.

[16] Kim, S. R.; Lee, H. Y. Integrative bioengineering strategies for endometrial regeneration: From biomaterials and stem cells to organoids and organ-on-a-chip technologies. *Theranostics* **2026**, *16*, 736–775. https://doi.org/10.7150/thno.123298.

[17] Munro, M. G.; Salazar, C. A.; Bhagavath, B.; Emanuel, M. H.; Huddleston, H. G.; Sobti, D.; et al. The epidemiology, clinical burden, and prevention of intrauterine adhesions (IUAs) related to surgically induced endometrial trauma: a systematic literature review and selective meta-analyses. *Hum. Reprod. Update* **2025**, *31*, 588–625. https://doi.org/10.1093/humupd/dmaf019.

[18] Rodríguez-Eguren, A.; Bueno-Fernandez, C.; Gómez-Álvarez, M. A.; Francés-Herrero, E.; Pellicer, A.; Bellver, J.; et al. Evolution of biotechnological advances and regenerative therapies for endometrial disorders: a systematic review. *Hum. Reprod. Update* **2024**, *30*, 584–613. https://doi.org/10.1093/humupd/dmae013.

[19] Lilly, K.; Agrawal, A.; Barik, B.; Gugulothu, S. B.; Rath, S. N.; Oh, S. J.; et al. Toward next-generation therapies for intrauterine adhesions: a perspective on granular hydrogel systems. *J. Mater. Chem. B* **2025**, *13*, 12869–12876. https://doi.org/10.1039/d5tb01624j.

[20] Zhao, G.; Hu, Y. Mechanistic insights into intrauterine adhesions. *Semin. Immunopathol.* **2025**, *47*, 3. https://doi.org/10.1007/s00281-024-01030-9.

[21] Dong, E.; Zhou, Z.; Chen, T.; Zhang, B.; Yin, Y.; Wu, X.; et al. Single-cell sequencing uncovers disrupted stromal-macrophage communication as a driver of intrauterine adhesion progression. *Commun. Biol.* **2025**, *8*, 1194. https://doi.org/10.1038/s42003-025-08634-3.

[22] Xia, S.; Ye, W.; Zeng, J.; Song, G.; Sun, Y.; Zhang, Y.; et al. A single-cell transcriptomic atlas of severe intrauterine adhesion. *MedComm Future Med.* **2024**, *3*, e70003. https://doi.org/10.1002/mef2.70003.

[23] Yang, J.; Li, J.; Wang, J.; Wu, J.; Yin, L.; Dou, H.; et al. Oroxylin A relieves intrauterine adhesion in mice through inhibiting macrophage pyroptosis via SIRT3-SOD2-ROS pathway. *Int. Immunopharmacol* **2023**, *118*, 110023. https://doi.org/10.1016/j.intimp.2023.110023.

[24] Yang, H.; Dou, C.; Pan, R.; Xu, Y.; Zeng, K.; Huang, J.; et al. Targeting Piezo1 can improve endometrial fibrosis by inhibiting ferroptosis in endothelial cells. *iScience* **2026**, *29*, 114540. https://doi.org/10.1016/j.isci.2025.114540.

[25] Yan, S.; Ding, J.; Wang, Z.; Zhang, Y.; Xu, Y.; Jia, Y.; et al. CTRP6 alleviates endometrial fibrosis by regulating Smad3 pathway in intrauterine adhesion. *Biol. Reprod.* **2024**, *111*, 322–331. https://doi.org/10.1093/biolre/ioae016.

[26] Zhou, Z.; Wang, H.; Zhang, X.; Song, M.; Yao, S.; Jiang, P.; et al. Defective autophagy contributes to endometrial epithelial-mesenchymal transition in intrauterine adhesions. *Autophagy* **2022**, *18*, 2427–2442. https://doi.org/10.1080/15548627.2022.2038994.

[27] Qin, X.; Zeng, B.; Sooranna, S.; Li, M. LAMB3 Promotes Myofibrogenesis and Cytoskeletal Reorganization in Endometrial Stromal Cells via the RhoA/ROCK1/MYL9 Pathway. *Cell Biochem. Biophys.* **2024**, *82*, 127–137. https://doi.org/10.1007/s12013-023-01186-5.

[28] Lv, H.; Nan, Z.; Jiang, P.; Wang, Z.; Song, M.; Ding, H.; et al. Vascular endothelial growth factor 165 inhibits pro-fibrotic differentiation of stromal cells via the DLL4/Notch4/smad7 pathway. *Cell Death Dis.* **2019**, *10*, 681. https://doi.org/10.1038/s41419-019-1928-z.

[29] Du, Y.; Shuai, R.; Luo, S.; Jin, Y.; Xu, F.; Zhang, J.; et al. Exploring the molecular mechanism of estrogen therapy effectiveness after TCRA in IUA patients at single-cell level. *Biol. Direct* **2024**, *19*, 142. https://doi.org/10.1186/s13062-024-00583-x.

[30] Cao, J.; Liu, D.; Zhao, S.; Yuan, L.; Huang, Y.; Ma, J.; et al. Estrogen attenuates TGF-β1-induced EMT in intrauterine adhesion by activating Wnt/β-catenin signaling pathway. *Braz. J. Med. Biol. Res.* **2020**, *53*, e9794. https://doi.org/10.1590/1414-431x20209794.

[31] Hinds, G. K.; Velieva, A.; Liu, J. Y.; Roy, A.; Chavali, R.; Loebel, C. Mechanical Cues Regulate Estrogen and Progesterone‐Induced Nascent ECM Deposition by Human Endometrial Stromal Fibroblasts. *J. Biomed. Mater. Res. A* **2026**, *114*, e70038. https://doi.org/10.1002/jbma.70038.

[32] Klunk, D.; Homewood, L.; Abebayehu, D. Extracellular matrix composition and stiffness regulates progesterone responsiveness and decidualization. *iScience* **2026**, *29*, 117009. https://doi.org/10.1016/j.isci.2026.117009.

[33] Sternberg, A. K.; Izmaylova, L.; Buck, V. U.; Classen-Linke, I.; Leube, R. E. An Assessment of the Mechanophysical and Hormonal Impact on

Under Review

Human Endometrial Epithelium Mechanics and Receptivity. *Int. J. Mol. Sci.* **2024**, *25*, 3726. https://doi.org/10.3390/ijms25073726.

[34] Gnecco, J. S.; Brown, A.; Buttrey, K.; Ives, C.; Goods, B. A.; Baugh, L.; Hernandez-Gordillo, V.; Loring, M.; Isaacson, K. B.; Griffith, L. G. Organoid co-culture model of the human endometrium in a fully synthetic extracellular matrix enables the study of epithelial-stromal crosstalk. *Med* **2023**, *4*, 554-579.e9. https://doi.org/10.1016/j.medj.2023.07.004.

[35] Rawlings, T. M.; Makwana, K.; Taylor, D. M.; Molè, M. A.; Fishwick, K. J.; Tryfonos, M.; Odendaal, J.; Hawkes, A.; Zernicka-Goetz, M.; Hartshorne, G. M.; et al. Modelling the impact of decidual senescence on embryo implantation in human endometrial assembloids. *eLife* **2021**, *10*, e69603. https://doi.org/10.7554/elife.69603.

[36] Tempest, N.; Hill, C. J.; Maclean, A.; Marston, K.; Powell, S. G.; Al-Lamee, H.; et al. Novel microarchitecture of human endometrial glands: implications in endometrial regeneration and pathologies. *Hum. Reprod. Update* **2022**, *28*, 153–171. https://doi.org/10.1093/humupd/dmab039.

[37] Xia, W.; Wang, Q.; Liu, M.; Lu, S.; Yu, H.; Yin, H.; et al. Antifouling and Injectable Granular Hydrogel for the Prevention of Postoperative Intrauterine Adhesion. *ACS Appl. Mater. Interfaces* **2023**, *15*, 44676–44688. https://doi.org/10.1021/acsami.3c07846.

[38] Abudukeyoumu, A.; Lai, Z. Z.; Lu, J. J.; Zhang, X.; Hou, D. Y.; Dong, J.; et al. A LIGHT-HVEM/LTβR axis contributes to the fibrosis of intrauterine adhesion. *J. Reprod. Immunol.* **2022**, *153*, 103693. https://doi.org/10.1016/j.jri.2022.103693.

[39] Feng, D.; Li, Y.; Zheng, H.; Wang, Y.; Deng, J.; Liu, T.; et al. IL-4-induced M2 macrophages inhibit fibrosis of endometrial stromal cells. *Reprod. Biol.* **2024**, *24*, 100852. https://doi.org/10.1016/j.repbio.2023.100852.

[40] Zhang, Z.; Li, S.; Deng, J.; Yang, S.; Xiang, Z.; Guo, H.; et al. Aspirin inhibits endometrial fibrosis by suppressing the TGF‐β1‐Smad2/Smad3 pathway in intrauterine adhesions. *Int. J. Mol. Med.* **2020**, *45*, 1351–1360. https://doi.org/10.3892/ijmm.2020.4506.

[41] Bao, M.; Feng, Q.; Zou, L.; Huang, J.; Zhu, C.; Xia, W. Endoplasmic reticulum stress promotes endometrial fibrosis through the TGF-β/SMAD pathway. *Reproduction* **2023**, *165*, 171–182. https://doi.org/10.1530/REP-22-0294.

[42] Xu, C.; Bao, M.; Fan, X.; Huang, J.; Zhu, C.; Xia, W. EndMT: New findings on the origin of myofibroblasts in endometrial fibrosis of intrauterine adhesions. *Reprod. Biol. Endocrinol.* **2022**, *20*, 9. https://doi.org/10.1186/s12958-022-00887-5.

[43] Cai, H.; Qiao, L.; Song, K.; He, Y. Oxidized, Regenerated Cellulose Adhesion Barrier Plus Intrauterine Device Prevents Recurrence After Adhesiolysis for Moderate to Severe Intrauterine Adhesions. *J. Minim. Invasive. Gynecol.* **2017**, *24*, 80–88. https://doi.org/10.1016/j.jmig.2016.09.021.

[44] Lee, K. B.; Chon, S. J.; Kim, S.; Kim, D. Y.; Park, C. W.; Shin, S. J.; et al. Using Type I Collagen Gel to Prevent Postoperative Intrauterine Adhesion: A Multicenter Retrospective Study. *J. Clin. Med.* **2023**, *12*, 3764. https://doi.org/10.3390/jcm12113764.

[45] Mao, X.; Tao, Y.; Cai, R.; Zhang, J.; Gao, H.; Chen, Q.; et al. Cross-linked hyaluronan gel to improve pregnancy rate of women patients with moderate to severe intrauterine adhesion treated with IVF: a randomized controlled trial. *Arch. Gynecol. Obstet.* **2020**, *301*, 199–205. https://doi.org/10.1007/s00404-019-05368-6.

[46] Salazar, C. A.; Chudnoff, S. G.; Roy, K. H.; Huddleston, H. G.; Bhagavath, B.; Movilla, P. R.; et al. Safety and effectiveness of an in situ-forming hydrogel barrier in preventing intrauterine adhesions after adhesiogenic hysteroscopic procedures: a multicenter, randomized, controlled trial. *Fertil. Steril.* **2026**. https://doi.org/10.1016/j.fertnstert.2026.07.015.

[47] Ciftci, B.; Karadag, B. Effectiveness of Hyaluronic Acid Gel in Preventing Postoperative Intrauterine Adhesion Formation Following Operative Hysteroscopy. *Int. J. Womens Health* **2026**, *18*, 609095. https://doi.org/10.2147/IJWH.S609095.

[48] Adiyeke, M.; Karaca, S. Y.; Ari, S. A.; Uyar, I.; Balcı, M. C. F.; Karaca, I. Hyaluronic Acid Barrier Gel for Preventing Adhesions After Hysteroscopic Myomectomy of Large Submucosal Myomas. *Int. J. Womens Health* **2026**, *18*, 587010. https://doi.org/10.2147/IJWH.S587010.

[49] Azumaguchi, A.; Henmi, H.; Saito, T. Efficacy of silicone sheet as a personalized barrier for preventing adhesion reformation after hysteroscopic adhesiolysis of intrauterine adhesions. *Reprod. Med. Biol.* **2019**, *18*, 378–383. https://doi.org/10.1002/rmb2.12294.

[50] Amer, M. I.; Abd-El-Maeboud, K. H. I.; Abdelfatah, I.; Salama, F. A.; Abdallah, A. S. Human amnion as a temporary biologic barrier after hysteroscopic lysis of severe intrauterine adhesions: pilot study. *J. Minim. Invasive. Gynecol.* **2010**, *17*, 605–611. https://doi.org/10.1016/j.jmig.2010.03.019.

[51] Shi, M.; Lin, J.; Wang, Q.; Yu, H.; You, M.; Chen, Q.; et al. Injectable, antifouling granular zwitterionic hydrogels for preventing postoperative intrauterine adhesion and restoring fertility. *Acta Biomater.* **2025**, *208*, 210–225. https://doi.org/10.1016/j.actbio.2025.10.053.

[52] Cai, Y.; Wu, F.; Yu, Y.; Liu, Y.; Shao, C.; Gu, H.; Li, M.; Zhao, Y. Porous scaffolds from droplet microfluidics for prevention of intrauterine adhesion. *Acta Biomater.* **2019**, *84*, 222-230. https://doi.org/10.1016/j.actbio.2018.11.016.

[53] Zhang, X.; Chen, G.; Wang, Y.; Fan, L.; Zhao, Y. Arrowhead Composite Microneedle Patches with Anisotropic Surface Adhesion for Preventing Intrauterine Adhesions. *Adv. Sci.* **2022**, *9*, e2104883. https://doi.org/10.1002/advs.202104883.

[54] Ding, Z.; Liang, Z.; Rong, X.; Fu, X.; Fan, J.; Lai, Y.; et al. Janus-Structured Microgel Barrier with Tissue Adhesive and Hemostatic Characteristics for Efficient Prevention of Postoperative Adhesion. *Small* **2024**, *20*, e2403753. https://doi.org/10.1002/smll.202403753.

[55] Lv, Y.; Cai, F.; Zhao, X.; Zhu, X.; Wei, F.; Zheng, Y.; Shi, X.; Yang, J. Bioinspired Microstructured Janus Bioadhesive for the Prevention of Abdominal and Intrauterine Adhesions. *Adv. Funct. Mater.* **2024**, *34*, 2314402. https://doi.org/10.1002/adfm.202314402.

[56] Liu, X.; Wang, H.; She, J.; Zhang, Q.; Hu, Q.; Li, D.; et al. An anti-fibroblast adhesion and anti-inflammatory hydrogel film combined with VEGF for intrauterine adhesion prevention. *Chem. Eng. J.* **2023**, *466*, 143144. https://doi.org/10.1016/j.cej.2023.143144.

[57] Xie, X.; Xu, R.; Ouyang, H.; Tan, S.; Guo, C.; Luo, X.; et al. A mechanically robust and stable estradiol-loaded PHEMA-based hydrogel barrier for intrauterine adhesion treatment. *J. Mater. Chem. B* **2022**, *10*, 8684–8695. https://doi.org/10.1039/d2tb01740g.

[58] Wang, Z.; Gu, Y.; Qu, Y.; Huang, X.; Sun, T.; Wu, W.; et al. Prevention of Intrauterine Adhesion with Platelet-Rich Plasma Double-Network Hydrogel. *Adv. Biol.* **2025**, *9*, e2400336. https://doi.org/10.1002/adbi.202400336.

[59] Lv, H.; Xu, R.; Xie, X.; Liang, Q.; Yuan, W.; Xia, Y.; et al. Injectable, degradable, and mechanically adaptive hydrogel induced by L-serine and allyl-functionalized chitosan with platelet-rich plasma for treating intrauterine adhesions. *Acta Biomater.* **2024**, *184*, 144–155. https://doi.org/10.1016/j.actbio.2024.06.043.

[60] Xie, X.; Ao, X.; Xu, R.; Lv, H.; Tan, S.; Wu, J.; et al. Injectable, stable, and biodegradable hydrogel with platelet-rich plasma induced by l-serine and sodium alginate for effective treatment of intrauterine adhesions. *Int. J. Biol. Macromol.* **2024**, *270*, 132363. https://doi.org/10.1016/j.ijbiomac.2024.132363.

[61] Zhang, W.; He, Y.; Chu, Y.; Zhai, Y.; Qian, S.; Wang, X.; et al. Amorphous curcumin-based hydrogels to reduce the incidence of post-surgical intrauterine adhesions. *Regen. Biomater.* **2024**, *11*, rbae043. https://doi.org/10.1093/rb/rbae043.

[62] Lin, J.; You, M.; Lv, X.; Mavhunure, V. V.; Wang, Q.; Tang, Z.; Yu, H.; Chen, Q.; Lin, F.; Hu, H. In Situ Click Chemistry Forming pH/ROS‐Responsive and Antifouling Hydrogel to Prevent Intrauterine Adhesion and Restore Fertility. *Adv. Healthc. Mater.* **2026**, *15*, e71444. https://doi.org/10.1002/adhm.71444.

[63] Wang, J.; Hu, Q.; Li, Y.; Yang, J.; Wu, L.; Zheng, J.; Qin, W.; Liu, S.; Zheng, L.; Qin, A.; et al. In-situ visible-light-crosslinking of mussel-inspired adhesive and anti-inflammatory HMD hydrogel for intrauterine adhesion prevention via paracrine signaling. *Adv. Compos. Hybrid Mater.* **2025**, *8*, 441. https://doi.org/10.1007/s42114-025-01536-2.

[64] Yu, S.; Zhang, X.; Li, W.; Lu, Y.; Xu, X.; Hu, R.; et al. Thermosensitive hydrogel as a sustained release carrier for mesenchymal

Just Accepted

stem cell-derived extracellular vesicles in the treatment of intrauterine adhesion. *J. Nanobiotechnology* **2024**, *22*, 570. https://doi.org/10.1186/s12951-024-02780-2.

[65] Li, J.; Pan, Y.; Yang, J.; Wang, J.; Jiang, Q.; Dou, H.; et al. Tumor necrosis factor-α-primed mesenchymal stem cell-derived exosomes promote M2 macrophage polarization via Galectin-1 and modify intrauterine adhesion on a novel murine model. *Front. Immunol.* **2022**, *13*, 945234. https://doi.org/10.3389/fimmu.2022.945234.

[66] Tang, L.; Li, Y.; Chen, S.; Zhao, X.; Jiang, S.; Jia, B.; Lu, Y. TNS1/TAGLN-enriched endometrial stromal cells is associated with a persistent fibrotic microenvironment in intrauterine adhesion. *Front. Cell Dev. Biol.* **2026**, *14*, 1810255. https://doi.org/10.3389/fcell.2026.1810255.

[67] Zan, J.; Shuai, Y.; Zhang, J.; Zhao, J.; Sun, B.; Yang, L. Hyaluronic acid encapsulated silver metal organic framework for the construction of a slow-controlled bifunctional nanostructure: Antibacterial and anti-inflammatory in intrauterine adhesion repair. *Int. J. Biol. Macromol.* **2023**, *230*, 123361. https://doi.org/10.1016/j.ijbiomac.2023.123361.

[68] Fan, G.; Lu, Y.; Li, Y.; Zhang, J.; Wang, Y.; Lee, P.; et al. Lactobacillus-Loaded Easily Injectable Hydrogel Promotes Endometrial Repair via Long-Term Retention and Microenvironment Modulation. *ACS Nano* **2025**, *19*, 4440–4451. https://doi.org/10.1021/acsnano.4c13593.

[69] Xiao, Q.; Ding, L.; Zhang, X.; Liu, C.; Li, Y.; Xu, R.; et al. Extracellular vesicles ameliorate intrauterine adhesion through Nrf2/GPX4-mediated ferroptosis suppression. *J. Adv. Res.* **2026**. https://doi.org/10.1016/j.jare.2026.02.035.

[70] Li, W.; Liao, C.; Li, Y.; Lin, Z.; Xiao, D.; Ye, G.; et al. A Reactive Oxygen Species-Responsive Biomimetic Adhesive Hydrogel Mediates Immunoregulation to Effectively Prevent Intrauterine Adhesions. *Pharmaceutics* **2026**, *18*, 685. https://doi.org/10.3390/pharmaceutics18060685.

[71] Cheng, P.; Song, J.; Li, Y.; Chen, M.; Liang, Z.; Qiu, B.; Liu, X.; Shi, X.; Fan, Y. An Injectable ROS‐Responsive Nanozyme Hydrogel Regulates the Uterine Microenvironment to Prevent Intrauterine Adhesions. *Adv. Sci.* **2026**, *e77510*. https://doi.org/10.1002/advs.77510.

[72] Wang, Z.; Ma, T.; Wan, D.; Chen, X.; Xu, Z.; Liang, S.; Fareed, M. S.; Li, M.; Ren, Y.; Ji, Q.; et al. Breaking the hemorrhage-ferroptosis-fibrosis axis: A ROS-responsive iron-trapping hydrogel remodels the local immune microenvironment for IUA therapy. *J. Control. Release* **2026**, *396*, 115092. https://doi.org/10.1016/j.jconrel.2026.115092.

[73] Li, M.; Zhu, R.; Tian, Y.; Yu, H.; Yang, L.; Wang, L. B.; et al. A thiol-rich immunomodulatory injectable hydrogel suppresses endometrial fibrosis to restore fertilization. *Sci. Adv.* **2026**, *12*, eaef5617. https://doi.org/10.1126/sciadv.aef5617.

[74] Wang, J.; Chen, Q.; Wang, Y.; Gan, Z.; Wu, M.; Shang, L.; et al. Multiresponsive Microcapsules for Prevention of Intrauterine Adhesion. *ACS Nano* **2025**, *19*, 6499–6510. https://doi.org/10.1021/acsnano.4c17645.

[75] Chen, K.; Wang, J.; Liu, Q.; Wang, H.; Ning, X.; Wang, J.; et al. Sodium hyaluronate based multifunctional hydrogels delivering SiRNA for sustained silencing of SMAD3: A novel strategy to treat intrauterine adhesions. *Carbohydr. Polym.* **2026**, *380*, 125123. https://doi.org/10.1016/j.carbpol.2026.125123.

[76] Ji, W.; Wen, J.; Tong, N.; Guo, F.; Zheng, J.; Wen, X.; et al. A pH-responsive hyaluronic acid hydrogel facilitates lesion-localized integrin α5β1 agonism to attenuate osteopontin signaling and fibrosis in intrauterine adhesions. *Acta Biomater.* **2026**, *214*, 156–176. https://doi.org/10.1016/j.actbio.2026.03.001.

[77] Zhang, D.; Li, L.; Zhou, J.; Wang, X.; Gao, X.; Chen, J.; Duan, T.; Ma, Q.; Li, J.; Yu, Y.; et al. Antifibrotic and antioxidant injectable hydrogel boosts endometrial repair and fertility via sGC/cGMP/SMAD7 signaling activation. *Chem. Eng. J.* **2025**, *512*, 162672. https://doi.org/10.1016/j.cej.2025.162672.

[78] Liang, Y.; Yu, Z.; Du, S.; Guo, Y.; Li, J.; Yan, Y.; et al. Decidualization-empowered ECM hydrogel integrating sustained Tβ4 release drives endometrial regeneration in intrauterine adhesions. *Nat. Commun.* **2026**, *17*, 1910. https://doi.org/10.1038/s41467-026-68677-w.

[79] Lin, S.; Shi, H.; Huang, X.; Chen, X.; Chen, L.; Zhan, Q.; Bai, S.; Shi, X.; Yang, J.; Chen, W. Micro–Nano Composite System Combining Mesenchymal Stem Cells and Pirfenidone for Endometrial Regeneration via Microenvironment Remodeling. *Adv. Healthc. Mater.* **2026**, *15*, e71466. https://doi.org/10.1002/adhm.71466.

[80] Wu, F.; Miao, Q.; Zhou, J.; Guo, R.; Chen, M.; Tong, N.; Zhao, Y.; Qiu, L.; Han, L.; Li, S.; et al. Therapeutic strategies: Bioactive hydrogels oxidized sodium alginate/strontium/betamethasone for preventing intrauterine adhesion. *Int. J. Biol. Macromol.* **2025**, *300*, 140220. https://doi.org/10.1016/j.ijbiomac.2025.140220.

[81] Chen, J. M.; Huang, Q. Y.; Chen, W. H.; Wu, J. X.; Zheng, L. T.; You, H. J.; Shi, Y. C.; Lin, S.; Shi, Q. R. Transcriptomics of tissue exosomes to investigate miR-195-5p's amelioration of endometrial fibrosis via the YAP-Smad7 pathway: an animal study. *J. Transl. Med.* **2024**, *22*, 1050. https://doi.org/10.1186/s12967-024-05871-8.

[82] Zhang, C.; Zhu, C.; Chen, X.; Chen, X.; Zhang, D.; Zhao, H.; Zhang, J.; Zhang, Y.; Xu, W.; Zhao, X.; et al. Natural regeneration-inspired sequential delivery of synergistic growth factors for structural and functional endometrial regeneration. *Acta Biomater.* **2025**, *201*, 121-138. https://doi.org/10.1016/j.actbio.2025.05.050.

[83] Lu, S.; Wang, X.; Li, W.; Zu, Y.; Xiao, J. Injectable 3D‐Printed Porous Scaffolds for Adipose Stem Cell Delivery and Endometrial Regeneration. *Adv. Funct. Mater.* **2023**, *33*, 2303368. https://doi.org/10.1002/adfm.202303368.

[84] Zhou, L.; Wang, H.; Shen, D.; Xiang, J.; Yu, N.; He, X.; et al. Stem cells implanted with nanofibrous mats for injured endometrial regeneration and immune-microenvironment remodeling. *Mater. Today Bio* **2023**, *23*, 100855. https://doi.org/10.1016/j.mtbio.2023.100855.

[85] Cai, H.; Wu, B.; Li, Y.; Liu, Y.; Shi, L.; Gong, L.; et al. Local Delivery of Silk-Cellulose Incorporated with Stromal Cell-Derived Factor-1alpha Functionally Improves the Uterus Repair. *Tissue Eng. Part A* **2019**, *25*, 1514–1526. https://doi.org/10.1089/ten.TEA.2018.0283.

[86] Xin, L.; Zheng, X.; Chen, J.; Hu, S.; Luo, Y.; Ge, Q.; et al. An Acellular Scaffold Facilitates Endometrial Regeneration and Fertility Restoration via Recruiting Endogenous Mesenchymal Stem Cells. *Adv. Healthc. Mater.* **2022**, *11*, e2201680. https://doi.org/10.1002/adhm.202201680.

[87] Ahn, J.; Sen, T.; Lee, D.; Kim, H.; Lee, J. Y.; Koo, H. S.; et al. Uterus‐Derived Decellularized Extracellular Matrix‐Mediated Endometrial Regeneration and Fertility Enhancement. *Adv. Funct. Mater.* **2023**, *33*, 2214291. https://doi.org/10.1002/adfm.202214291.

[88] Zhang, H.; Zhang, Q.; Zhang, J.; Sheng, F.; Wu, S.; Yang, F.; et al. Urinary bladder matrix scaffolds improve endometrial regeneration in a rat model of intrauterine adhesions. *Biomater. Sci.* **2020**, *8*, 988–996. https://doi.org/10.1039/c9bm00651f.

[89] Li, X.; Li, P.; Wang, C.; Shang, T.; Han, H.; Tong, Y.; et al. A thermo-sensitive and injectable hydrogel derived from a decellularized amniotic membrane to prevent intrauterine adhesion by accelerating endometrium regeneration. *Biomater. Sci.* **2022**, *10*, 2275–2286. https://doi.org/10.1039/d1bm01791h.

[90] Zhao, H.; He, S.; Zhang, W.; Yu, M.; Bao, H. Degradable Endometrial Repair Membrane (DERM) promoted the endometrial regeneration in intrauterine adhesions therapy. Biol. Reprod. 2026, ioag151. https://doi.org/10.1093/biolre/ioag151.

[91] Cao, Y.; Qi, J.; Wang, J.; Chen, L.; Wang, Y. Injectable "Homing-Like" Bioactive Short-Fibers for Endometrial Repair and Efficient Live Births. *Adv. Sci.* **2024**, *11*, e2306507. https://doi.org/10.1002/advs.202306507.

[92] Nie, N.; Gong, L.; Jiang, D.; Liu, Y.; Zhang, J.; Xu, J.; et al. 3D bio-printed endometrial construct restores the full-thickness morphology and fertility of injured uterine endometrium. *Acta Biomater.* **2023**, *157*, 187–199. https://doi.org/10.1016/j.actbio.2022.12.016.

[93] Ji, W.; Hou, B.; Lin, W.; Wang, L.; Zheng, W.; Li, W.; et al. 3D Bioprinting a human iPSC-derived MSC-loaded scaffold for repair of the uterine endometrium. *Acta Biomater.* **2020**, *116*, 268–284. https://doi.org/10.1016/j.actbio.2020.09.012.

[94] Park, S. R.; Kim, S. R.; Im, J. B.; Park, C. H.; Lee, H. Y.; Hong, I. S. 3D stem cell-laden artificial endometrium: successful endometrial regeneration and pregnancy. *Biofabrication* **2021**, *13*, 045012. https://doi.org/10.1088/1758-5090/ac165a.

Just Accepted

[95] Gómez-Álvarez, M. A.; Bueno-Fernandez, C.; Francés-Herrero, E.; Agustina-Hernández, M.; Alonso-Frías, P.; Corpas, N.; et al. Hybrid endometrial-derived hydrogel and human endometrial organoids synergize for uterine regeneration in an immunocompetent murine model. *Stem Cell Res. Ther.* **2026**, *17*, 79. https://doi.org/10.1186/s13287-026-04900-1.

[96] You, S.; Liu, S.; Shi, X.; Hu, L. Injectable decellularized endometrium extracellular matrix/chitosan hydrogels improved the endometrium regeneration and fertility restoration. *Mater. Des.* **2026**, *269*, 116607. https://doi.org/10.1016/j.matdes.2026.116607.

[97] Hernandez-Gordillo, V.; Kassis, T.; Lampejo, A.; Choi, G.; Gamboa, M. E.; Gnecco, J. S.; Brown, A.; Breault, D. T.; Carrier, R.; Griffith, L. G. Fully synthetic matrices for in vitro culture of primary human intestinal enteroids and endometrial organoids. *Biomaterials* **2020**, *254*, 120125. https://doi.org/10.1016/j.biomaterials.2020.120125.

[98] Dai, Y.; Zhao, F.; Chen, Q.; Zeng, B.; Gu, W.; Zhang, Y.; Sun, F.; Wang, X.; Lin, X.; Liu, N.; et al. Microfluidic chip-integrated vascularized endometrial complexes: Mitochondrial function and paracrine crosstalk enhance regenerative potential. *Bioact. Mater.* **2025**, *54*, 551-569. https://doi.org/10.1016/j.bioactmat.2025.08.035.

[99] Xu, Y.; Cai, S.; Wang, Q.; Cheng, M.; Hui, X.; Dzakah, E. E.; Zhao, B.; Chen, X. Multi-Lineage Human Endometrial Organoids on Acellular Amniotic Membrane for Endometrium Regeneration. *Cell Transplant.* **2023**, *32*, 09636897231218408. https://doi.org/10.1177/09636897231218408.

[100] Zhang, S.; Chang, Q.; Li, P.; Tong, X.; Feng, Y.; Hao, X.; et al. Concentrated small extracellular vesicles from menstrual blood-derived stromal cells improve intrauterine adhesion, a pre-clinical study in a rat model. *Nanoscale* **2021**, *13*, 7334–7347. https://doi.org/10.1039/d0nr08942g.

[101] Lin, J.; Wang, Z.; Huang, J.; Tang, S.; Saiding, Q.; Zhu, Q.; et al. Microenvironment-Protected Exosome-Hydrogel for Facilitating Endometrial Regeneration, Fertility Restoration, and Live Birth of Offspring. *Small* **2021**, *17*, e2007235. https://doi.org/10.1002/smll.202007235.

[102] Jin, X.; Dai, Y.; Xin, L.; Ye, Z.; Chen, J.; He, Q.; et al. ADSC-derived exosomes-coupled decellularized matrix for endometrial regeneration and fertility restoration. *Mater. Today Bio* **2023**, *23*, 100857. https://doi.org/10.1016/j.mtbio.2023.100857.

[103] Xin, L.; Lin, X.; Zhou, F.; Li, C.; Wang, X.; Yu, H.; et al. A scaffold laden with mesenchymal stem cell-derived exosomes for promoting endometrium regeneration and fertility restoration through macrophage immunomodulation. *Acta Biomater.* **2020**, *113*, 252–266. https://doi.org/10.1016/j.actbio.2020.06.029.

[104] Zhang, Y.; Liang, L.; Ma, K.; Li, F.; Kong, L.; He, R.; et al. An Injectable Clinical-Grade Fibrin Hydrogel Restores Fertility in Intrauterine Adhesions via MSC-Mediated Immune and Regenerative Modulation, Unlocking an Equivalent Cell-Free EV-Based Therapy. *Adv. Healthc. Mater.* **2026**, *15*, e04360. https://doi.org/10.1002/adhm.202504360.

[105] Yang, H.; Xie, J.; Zhan, J.; Li, M.; Zhang, Y.; Liu, B.; et al. Bioprinted Human Umbilical Cord Mesenchymal Stem Cell-laden Microfiber-derived Extracellular Vesicles Promote Endometrial Repair and Fertility Recovery in Intrauterine Adhesions. *Stem Cell Rev. Rep.* **2026**, *22*, 2902–2918. https://doi.org/10.1007/s12015-026-11165-x.

[106] Lin, X.; Fang, Y.; Mi, X.; Fu, J.; Chen, S.; Wu, M.; et al. Intrauterine injection of bioengineered hydrogel loaded exosomes derived from HUCM stem cells and spermidine prominently augments the pregnancy rate in thin endometrium rats. *Regen. Ther.* **2024**, *27*, 63–72. https://doi.org/10.1016/j.reth.2024.02.003.

[107] Xin, L.; Wei, C.; Tong, X.; Dai, Y.; Huang, D.; Chen, J.; et al. In situ delivery of apoptotic bodies derived from mesenchymal stem cells via a hyaluronic acid hydrogel: A therapy for intrauterine adhesions. *Bioact. Mater.* **2022**, *12*, 107–119. https://doi.org/10.1016/j.bioactmat.2021.10.025.

[108] Welsh, J. A.; Goberdhan, D. C. I.; O'Driscoll, L.; Buzas, E. I.; Blenkiron, C.; Bussolati, B.; et al. Minimal information for studies of extracellular vesicles (MISEV2023): From basic to advanced approaches. *J. Extracell. Vesicles* **2024**, *13*, e12404. https://doi.org/10.1002/jev2.12404.

[109] Wang, L.; Yu, C.; Chang, T.; Zhang, M.; Song, S.; Xiong, C.; et al. In situ repair abilities of human umbilical cord-derived mesenchymal stem cells and autocrosslinked hyaluronic acid gel complex in rhesus monkeys with intrauterine adhesion. *Sci. Adv.* **2020**, *6*, eaba6357. https://doi.org/10.1126/sciadv.aba6357.

[110] Fan, J.; Xie, J.; Liao, Y.; Lai, B.; Zhou, G.; Lian, W.; et al. Human umbilical cord-derived mesenchymal stem cells and auto-crosslinked hyaluronic acid gel complex for treatment of intrauterine adhesion. *Aging* **2024**, *16*, 6273–6289. https://doi.org/10.18632/aging.205704.

[111] Zhang, D.; Du, Q.; Li, C.; Ding, C.; Chen, J.; He, Y.; et al. Functionalized human umbilical cord mesenchymal stem cells and injectable HA/Gel hydrogel synergy in endometrial repair and fertility recovery. *Acta Biomater.* **2023**, *167*, 205–218. https://doi.org/10.1016/j.actbio.2023.06.013.

[112] Feng, M.; Hu, S.; Qin, W.; Tang, Y.; Guo, R.; Han, L. Bioprinting of a Blue Light-Cross-Linked Biodegradable Hydrogel Encapsulating Amniotic Mesenchymal Stem Cells for Intrauterine Adhesion Prevention. *ACS Omega* **2021**, *6*, 23067–23075. https://doi.org/10.1021/acsomega.1c02117.

[113] Han, X.; Ma, Y.; Lu, X.; Li, W.; Xia, E.; Li, T. C.; et al. Transplantation of Human Adipose Stem Cells Using Acellular Human Amniotic Membrane Improves Angiogenesis in Injured Endometrial Tissue in a Rat Intrauterine Adhesion Model. *Cell Transplant.* **2020**, *29*, 963689720952055. https://doi.org/10.1177/0963689720952055.

[114] Liu, Y.; Cai, J.; Luo, X.; Wen, H.; Luo, Y. Collagen Scaffold with Human Umbilical Cord Mesenchymal Stem Cells Remarkably Improves Intrauterine Adhesions in a Rat Model. *Gynecol. Obstet. Invest.* **2020**, *85*, 267–276. https://doi.org/10.1159/000505691.

[115] Kim, Y. Y.; Park, K. H.; Kim, Y. J.; Kim, M. S.; Liu, H. C.; Rosenwaks, Z.; et al. Synergistic regenerative effects of functionalized endometrial stromal cells with hyaluronic acid hydrogel in a murine model of uterine damage. *Acta Biomater.* **2019**, *89*, 139–151. https://doi.org/10.1016/j.actbio.2019.03.032.

[116] Song, Y.; Ma, R.; Yi, B.; Zhou, Q.; Li, X.; Zhou, Y.; et al. Microfluidic 3D-printed MSC-laden bioactive hydrogel for intrauterine adhesion prevention and endometrial regeneration. *Mater. Today Bio* **2026**, *36*, 102742. https://doi.org/10.1016/j.mtbio.2025.102742.

[117] Liu, Q.; Lu, S.; Zhou, J.; Xu, J.; Shao, J.; Zheng, J.; et al. A sequential and synergistic release sacrificial microgels scaffold for endometrial niche reprogramming and fertility restoration. *Mater. Today Bio* **2026**, *38*, 103235. https://doi.org/10.1016/j.mtbio.2026.103235.

[118] Zhang, S. S.; Xu, X. X.; Xiang, W. W.; Zhang, H. H.; Lin, H. L.; Shen, L. E.; et al. Using 17beta-estradiol heparin-poloxamer thermosensitive hydrogel to enhance the endometrial regeneration and functional recovery of intrauterine adhesions in a rat model. *FASEB J.* **2020**, *34*, 446–457. https://doi.org/10.1096/fj.201901603RR.

[119] Yao, Q.; Zheng, Y. W.; Lan, Q. H.; Wang, L. F.; Huang, Z. W.; Chen, R.; et al. Aloe/poloxamer hydrogel as an injectable β-estradiol delivery scaffold with multi-therapeutic effects to promote endometrial regeneration for intrauterine adhesion treatment. *Eur. J. Pharm. Sci.* **2020**, *148*, 105316. https://doi.org/10.1016/j.ejps.2020.105316.

[120] Chen, Y.; Fei, W.; Zhao, Y.; Wang, F.; Zheng, X.; Luan, X.; et al. Sustained delivery of 17beta-estradiol by human amniotic extracellular matrix (HAECM) scaffold integrated with PLGA microspheres for endometrium regeneration. *Drug Deliv.* **2020**, *27*, 1165–1175. https://doi.org/10.1080/10717544.2020.1801891.

[121] Guan, C. Y.; Wang, F.; Zhang, L.; Sun, X. C.; Zhang, D.; Wang, H.; et al. Genetically engineered FGF1-sericin hydrogel material treats intrauterine adhesion and restores fertility in rat. *Regen. Biomater.* **2022**, *9*, rbac016. https://doi.org/10.1093/rb/rbac016.

[122] Wen, J.; Hou, B.; Lin, W.; Guo, F.; Cheng, M.; Zheng, J.; et al. 3D-printed hydrogel scaffold-loaded granulocyte colony-stimulating factor sustained-release microspheres and their effect on endometrial regeneration. *Biomater. Sci.* **2022**, *10*, 3346–3358. https://doi.org/10.1039/d2bm00109h.

[123] López-Martínez, S.; Rodríguez-Eguren, A.; de Miguel-Gómez, L. A.; Francés-Herrero, E.; Faus, A.; Díaz, A.; et al. Bioengineered endometrial

Just Accepted

hydrogels with growth factors promote tissue regeneration and restore fertility in murine models. *Acta Biomater.* **2021**, *135*, 113–125. https://doi.org/10.1016/j.actbio.2021.08.025.

[124] Cao, Y.; Sun, H.; Zhu, H.; Zhu, X.; Tang, X.; Yan, G.; et al. Allogeneic cell therapy using umbilical cord MSCs on collagen scaffolds for patients with recurrent uterine adhesion: a phase I clinical trial. *Stem Cell Res. Ther.* **2018**, *9*, 192. https://doi.org/10.1186/s13287-018-0904-3.

[125] Zhang, Y.; Shi, L.; Lin, X.; Zhou, F.; Xin, L.; Xu, W.; et al. Unresponsive thin endometrium caused by Asherman syndrome treated with umbilical cord mesenchymal stem cells on collagen scaffolds: a pilot study. *Stem Cell Res. Ther.* **2021**, *12*, 420. https://doi.org/10.1186/s13287-021-02499-z.

[126] Hanuman, S.; B, H. K.; Pai, K. S. R.; Nune, M. Surface-Conjugated Galactose on Electrospun Polycaprolactone Nanofibers: An Innovative Scaffold for Uterine Tissue Engineering. *ACS Omega* **2024**, *9*, 34314-34328. https://doi.org/10.1021/acsomega.3c10445.

[127] Chaudhuri, O.; Gu, L.; Klumpers, D.; Darnell, M.; Bencherif, S. A.; Weaver, J. C.; Huebsch, N.; Lee, H. P.; Lippens, E.; Duda, G. N.; et al. Hydrogels with tunable stress relaxation regulate stem cell fate and activity. *Nat. Mater.* **2015**, *15*, 326-334. https://doi.org/10.1038/nmat4489.

[128] Zhu, H.; Li, H.; Gao, K.; Huang, Y.; Liao, Y.; Hu, W.; et al. Chorionic villi-derived nanofibers enhanced mesenchymal stem cell extracellular vesicle secretion and bioactivity for endometrium regeneration toward intrauterine adhesion treatment. *Nano Today* **2023**, *52*, 101986. https://doi.org/10.1016/j.nantod.2023.101986.

[129] International Organization for Standardization. Biological evaluation of medical devices — Part 1: Requirements and general principles for the evaluation of biological safety within a risk management process (*ISO* **1099**3-1:2025). ISO. 2025. https://www.iso.org/standard/10993-1.

[130] International Organization for Standardization. Biological evaluation of medical devices — Part 3: Evaluation of genotoxicity, carcinogenicity, reproductive toxicity and developmental toxicity (*ISO* **1099**3-3:2026). ISO. 2026. https://www.iso.org/standard/88199.html.

[131] International Council for Harmonisation of Technical Requirements for Pharmaceuticals for Human Use. Detection of reproductive and developmental toxicity for human pharmaceuticals S5(R3). ICH. 2020. https://database.ich.org/sites/default/files/S5-R3_Step4_Guideline_2020_0218_1.pdf.

[132] Ji, W.; Wen, J.; Lin, W.; He, P.; Hou, B.; Quan, S. Comparing the Characteristics of Amniotic Membrane-, Endometrium-, and Urinary-Derived ECMs and Their Effects on Endometrial Regeneration in a Rat Uterine Injury Model. *Front. Bioeng. Biotechnol.* **2022**, *10*, 861496. https://doi.org/10.3389/fbioe.2022.861496.

[133] Peng, X.; Wang, T.; Dai, B.; Zhu, Y.; Ji, M.; Yang, P.; et al. Gene Therapy for Inflammatory Cascade in Intrauterine Injury with Engineered Extracellular Vesicles Hybrid Snail Mucus-enhanced Adhesive Hydrogels. *Adv. Sci.* **2025**, *12*, e2410769. https://doi.org/10.1002/advs.202410769.

[134] Fu, W.; Qian, K.; Ai, H.; Zou, Y.; Zhou, Y.; Mao, R.; et al. Development of CAR Exosomes Targeting FAP for the Treatment of Intrauterine Adhesion. *J. Extracell. Vesicles* **2026**, *15*, e70284. https://doi.org/10.1002/jev2.70284.

Just Accepted